Applied Energy 305 (2022) 117700

Contents lists available at ScienceDirect

Applied Energy

journal homepage: www.elsevier.com/locate/apenergy

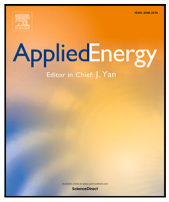

Assessing the impact of offshore wind siting strategies on the design of the European power system

David Radu [a,*], Mathias Berger [a], Antoine Dubois [a], Raphaël Fonteneau [a], Hrvoje Pandžić [b], Yury Dvorkin [c], Quentin Louveaux [a], Damien Ernst [a]

[a] Department of Electrical Engineering and Computer Science, University of Liège, Allée de la Découverte 10, 4000 Liège, Belgium
[b] Faculty of Electrical Engineering and Computing, University of Zagreb, HR-1000 Zagreb, Croatia
[c] Department of Electrical and Computer Engineering, NYU Tandon School of Engineering, NY 11201, USA

ARTICLE INFO

Keywords:
Asset siting
Two-stage method
Offshore wind
Resource complementarity
Capacity expansion planning

ABSTRACT

This paper provides a detailed account of the impact of different offshore wind siting strategies on the design of the European power system. To this end, a two-stage method is proposed. In the first stage, a highly-granular siting problem identifies a suitable set of sites where offshore wind plants could be deployed according to a pre-specified criterion. Two siting schemes are analysed and compared within a realistic case study. These schemes essentially select a pre-specified number of sites so as to maximize their aggregate power output and their spatiotemporal complementarity, respectively. In addition, two variants of these siting schemes are provided, wherein the number of sites to be selected is specified on a country-by-country basis rather than Europe-wide. In the second stage, the subset of previously-identified sites is passed to a capacity expansion planning framework that sizes the power generation, transmission and storage assets that should be deployed and operated in order to satisfy pre-specified electricity demand levels at minimum cost. Results show that the complementarity-based siting criterion leads to system designs which are up to 5% cheaper than the ones relying on the power output-based scheme when offshore wind plants are deployed with no consideration for country-based deployment targets. On the contrary, the power output-based scheme leads to system designs which are consistently 2% cheaper than the ones leveraging the complementarity-based siting strategy when such constraints are enforced. The robustness of the reported results is supported by a sensitivity analysis on offshore wind capital expenditure and inter-annual weather variability, respectively.

1. Introduction

The large-scale deployment of technologies harnessing renewable energy sources (RES) for electricity production has been a mainstay of climate and decarbonization policies. In Europe, solar photovoltaic and onshore wind power plants have formed the bulk of new renewable capacity additions for over a decade [1]. Nevertheless, in spite of the need for extra capacity deployments required to achieve ambitious decarbonization targets [2], the pace at which these technologies are being deployed in a number of countries has remained sluggish of late [1], often as a result of social acceptance issues [3] and the phasing out of renewable support schemes. On the other hand, the economics of offshore wind power generation have greatly improved in recent years [4]. Offshore wind power plants are also located in unpopulated areas and are therefore less subject to social acceptance issues than onshore ones. Furthermore, the offshore wind resource is most often of much better quality than the onshore one [5]. Hence, the large-scale deployment of offshore wind power plants has increasingly been viewed as a key enabler of European decarbonization efforts [6,7].

However, widely-available RES such as solar irradiance or offshore wind are inherently variable on time scales ranging from minutes to years and integrating them in power systems typically complicates planning and operational procedures [8]. Several solutions have been advocated to alleviate these issues, including the large-scale deployment of electricity storage systems [9,10] or the implementation of demand response programs [11]. Alternatively, since RES are heterogeneously-distributed in space and time, it has been suggested that siting RES electricity production assets so as to exploit this diversity may reduce the aggregate output variability of RES power plants as well as the residual electricity load (i.e., total load minus renewable production) [12,13]. The concept of RES complementarity formalizes this idea [14].

* Corresponding author.
E-mail address: dcradu@uliege.be (D. Radu).

https://doi.org/10.1016/j.apenergy.2021.117700
Received 8 February 2021; Received in revised form 18 August 2021; Accepted 23 August 2021

Nomenclature

Acronyms

AC	Alternate Current
ASC	Annualized (Total) System Cost
CAPEX	Capital Expenditure
CEP	Capacity Expansion Planning
DC	Direct Current
EEZ	Exclusive Economic Zone
FOM	Fixed Operation and Maintenance Cost
GW	Gigawatt
IEC	International Electrotechnical Commission
IP	Integer Program
LP	(Continuous) Linear Program
MILP	Mixed-Integer Linear Program
MIR	Mixed-Integer Relaxation
PHS	Pumped-Hydro Storage
PV	Photovoltaic
RES	Renewable Energy Sources
TWh	Terawatt-hour
TYNDP	Ten-Year Network Development Plan
VOM	Variable Operation and Maintenance Cost

Indices & Sets

c	Transmission corridor index
d	Index of technology providing firm generation capacity
g	Dispatchable generation technology index
l	RES site
n	Topology node
r	RES technology index
s	Storage technology index
t	Time period index
w	Time window index
$\mathcal{C}$	Set of transmission corridors, $\mathcal{C} \subset \mathcal{N}_B \times \mathcal{N}_B$
$\mathcal{C}_n^+, \mathcal{C}_n^-$	Set of inbound (outbound) links into (from) node n
$\mathcal{D}$	Set of technologies providing firm generation capacity
$\mathcal{G}$	Set of dispatchable generation technologies, with $\mathcal{G} \subseteq \mathcal{D}$
$\mathcal{L}$	Set of candidate RES sites
$\mathcal{L}_n$	Set of candidate RES sites in partition $n \in \mathcal{N}_B$
$\mathcal{L}_0$	Set of legacy RES sites
L_n	Set of selected RES sites associated with $n \in \mathcal{N}_B$
$\mathcal{N}_B$	Set of topology nodes
$\mathcal{R}$	Set of RES technologies
$\mathcal{S}$	Set of storage technologies
$\mathcal{T}$	Set of time periods
$\mathcal{W}$	Set of time windows

Parameters

$\alpha_{l\mathrm{w}}$	Reference production level at location l during time window w
δ	Time window duration
Δ_g^+	Upward ramp-rate of dispatchable technology $g \in \mathcal{G}$
Δ_g^-	Downward ramp-rate of dispatchable technology $g \in \mathcal{G}$
ϵ_{site}	Reference site surface utilization factor
ζ^j	Annualized investment cost of tech. $j \in \{\mathcal{G}, \mathcal{R}, \mathcal{S}, \mathcal{C}\}$
ζ^l	Annualized investment cost at RES site $l \in \mathcal{L}$
ζ_S^s	Annualized investment cost of the energy component of storage technology $s \in \mathcal{S}$
η_s^C	Discharge efficiency of storage technology $s \in \mathcal{S}$
η_s^D	Charge efficiency of storage technology $s \in \mathcal{S}$
η_s^{SD}	Self-discharge efficiency of storage technology $s \in \mathcal{S}$
η_g	Thermal efficiency of generation technology $g \in \mathcal{G}$
θ_f^j	FOM cost of technology $j \in \{\mathcal{G}, \mathcal{R}, \mathcal{S}, \mathcal{C}\}$
θ_v^j	VOM cost of technology $j \in \{\mathcal{G}, \mathcal{R}, \mathcal{S}, \mathcal{C}\}$
θ_f^l	FOM cost of RES site $l \in \mathcal{L}$
θ_v^l	VOM cost of RES site $l \in \mathcal{L}$
θ^{ens}	Economic penalty for demand curtailment
κ_n	Target installed capacity at partition $\mathcal{L}_n$
$\underline{\kappa}_c$	Initial capacity for transmission line $c \in \mathcal{C}$
$\underline{\kappa}_l$	Initial capacity at site $l \in \mathcal{L}$
$\underline{\kappa}_{nx}$	Initial capacity for technology $x \in \{\mathcal{G}, \mathcal{R}, \mathcal{S}\}$ at node $n \in \mathcal{N}_B$
$\bar{\kappa}_c$	Maximum allowable capacity of line $c \in \mathcal{C}$
$\bar{\kappa}_l$	Maximum allowable capacity at site $l \in \mathcal{L}$
$\bar{\kappa}_{nx}$	Maximum allowable capacity of technology $x \in \{\mathcal{G}, \mathcal{R}, \mathcal{S}\}$ at node $n \in \mathcal{N}_B$
$\bar{\lambda}_w$	System-wide electricity demand during time window w
λ_{nt}	Electricity demand at node n and time t
$\hat{\lambda}_n$	Peak electricity demand at node n
μ_j	Minimum operational level of technology $j \in \{\mathcal{G}, \mathcal{S}\}$
$\nu_g^{CO_2}$	Specific CO_2 emissions associated with generation technology $g \in \mathcal{G}$
π_{lt}	Per-unit availability of RES site l and time step t
$\bar{\pi}_{l\mathrm{w}}$	Per-unit availability of RES site $l \in \mathcal{L}$ during time window $\mathrm{w} \in \mathcal{W}$
$\tilde{\pi}_l$	Average per-unit availability of RES site $l \in \mathcal{L}$
Π_l	Capacity credit of RES site $l \in \mathcal{L}$
Π_{nr}	Capacity credit of technology $r \in \mathcal{R}$ at node $n \in \mathcal{N}_B$
ρ_r	Power density of RES technology $r \in \mathcal{R}$
σ_{site}	Reference site surface area
ς	Dimensionless parameter representing the share of yearly demand covered by the sited RES technologies
ϕ_s	Charge-to-discharge ratio of storage technology $s \in \mathcal{S}$
Φ_n	Planning reserve margin at node $n \in \mathcal{N}_B$
Ψ^{CO_2}	System-wide CO_2 budget
ω_s	Weight of each operating condition $t \in \mathcal{T}$ in the operation of storage units
ω_t	Weight of each operating condition $t \in \mathcal{T}$ in the objective function and CO_2 emissions

From a modelling perspective, the interplay between investment (both siting and sizing) and operational decisions should be accounted for in order to evaluate the impact of siting strategies on system design and economics. Hence, ideally, models should perform both siting and sizing simultaneously, have a high spatiotemporal resolution as well as a high level of technical detail. Unfortunately, such models quickly become impractical (e.g., require tens of thousands of core-hours [15]) or intractable. Thus, the siting and sizing problems have traditionally been tackled separately in the literature, but the outcomes of siting models have rarely been leveraged in sizing models.

In this paper, the role that offshore wind power plants may play in the European power system is analysed, with a particular focus on the impact that plant siting strategies have on system design and economics. To this end, a two-stage method is developed. In the first stage, a highly-granular siting problem is solved in order to identify a suitable subset of candidate sites where offshore wind power plants could be deployed. Then, in the second stage, the subset of locations

A_{nl}	Incidence matrix entry indicating whether location l belongs to partition $\mathcal{L}_n$
c	Threshold (i.e., number of sites) defining the global coverage of time windows
$D_{l\mathrm{w}}$	Criticality matrix entry indicating whether location l covers time window w
g_l	Resource assessment measure at location l
h_l	RES transfer function at location l
I	Iterations in the simulated annealing (SA) algorithm
k_n	Number of desired deployments in partition $\mathcal{L}_n$
N	Number of neighbouring solutions in the SA algorithm
r	Neighbourhood radius in the SA algorithm
s_{lt}	Renewable resource (e.g., wind speed) at location l and time step $t \in \mathcal{T}$
$T(i)$	Annealing schedule (function of iteration i)

Variables

$e_{nst} \in \mathbb{R}_+$	state of charge of storage technology $s \in \mathcal{S}$ at node $n \in \mathcal{N}_B$ and time $t \in \mathcal{T}$
$K_c \in \mathbb{R}_+$	Installed capacity of transmission line $c \in \mathcal{C}$
$K_l \in \mathbb{R}_+$	Installed capacity of RES site $l \in \mathcal{L}$
$K_{nj} \in \mathbb{R}_+$	Installed capacity of generation technology $j \in \{\mathcal{G}, \mathcal{R}\}$ at node $n \in \mathcal{N}_B$
$K_{ns} \in \mathbb{R}_+$	Power capacity of storage technology $s \in \mathcal{S}$
$p^C_{nst} \in \mathbb{R}_+$	Charging flow of storage technology $s \in \mathcal{S}$, at node $n \in \mathcal{N}_B$ and time $t \in \mathcal{T}$
$p^D_{nst} \in \mathbb{R}_+$	Discharging flow of storage technology $s \in \mathcal{S}$, at node $n \in \mathcal{N}_B$ and time $t \in \mathcal{T}$
$p^{ens}_{nt} \in \mathbb{R}_+$	Unserved demand at node $n \in \mathcal{N}_B$ and time step $t \in \mathcal{T}$
$p_{ct} \in \mathbb{R}$	Power flow over line $l \in \mathcal{C}$ at time $t \in \mathcal{T}$
$p_{lt} \in \mathbb{R}_+$	Feed-in of RES site $l \in L_n$ at time $t \in \mathcal{T}$
$p_{ngt} \in \mathbb{R}_+$	Feed-in of generation technology $g \in \mathcal{G}$, at node $n \in \mathcal{N}_B$ and time $t \in \mathcal{T}$
$q^{CO_2}_{ngt} \in \mathbb{R}_+$	CO_2 emissions from the operation of technology $g \in \mathcal{G}$ at node $n \in \mathcal{N}_B$ and time step $t \in \mathcal{T}$
$S_{ns} \in \mathbb{R}_+$	Energy capacity of storage technology $s \in \mathcal{S}$
$x_l \in \{0,1\}$	Variable indicating deployment of site $l \in \mathcal{L}$
$y_w \in \{0,1\}$	Variable indicating the system-wide criticality of window $w \in \mathcal{W}$

selected in the first stage is passed to a capacity expansion planning framework that sizes the power generation, transmission and storage assets that should be deployed and operated in order to satisfy pre-specified electricity demand levels at minimum cost subject to technical and policy constraints. An open source tool implementing the two-stage method is also provided for the sake of transparency [16,17].

Two types of deployment schemes that select sites so as to maximize their aggregate power output and spatiotemporal complementarity, respectively, are analysed. Roughly speaking, sites are considered complementary if they rarely experience simultaneous low electricity production events [18]. Two variants of these siting schemes are also studied, wherein the number of sites to be selected is specified on a country-by-country basis rather than Europe-wide. A few hundred sites are identified using each scheme, by leveraging a high resolution grid and ten years of reanalysis data [19]. These sites are then passed to a capacity expansion planning framework relying on a stylized model of the European power system where each country corresponds to an electrical bus and including an array of power generation and storage technologies. The framework sizes gas-fired power plants, offshore wind power plants, battery storage and electricity transmission assets and operates the system so as to supply electricity demand levels consistent with current European electricity consumption at minimum cost while reducing carbon dioxide emissions from the power sector by 90% compared with 1990 levels and taking a broad range of legacy assets into account. A detailed sensitivity analysis is also performed in order to evaluate the impact of offshore wind cost assumptions and inter-annual weather variability on system design and economics.

This manuscript is organized as follows. Section 2 reviews the relevant studies in the literature. Section 3 presents the two-stage method used to evaluate the impact of RES siting strategies on power system design and economics. The case study is introduced in Section 4, while results are presented and analysed in Section 5. Section 6 concludes the paper and discusses future work avenues.

2. Related works

The precise estimation of required capacities and incurred costs in RES-dominated power systems relies heavily on the detailed modelling of RES assets [20]. In one of the first studies quantifying the impact of this modelling aspect, Krishnan and Cole [21] reveal that using 356 and 134 profiles to model the wind and solar resource, respectively, within the contiguous USA leads to significantly different capacity outcomes compared to the case where the same resources are modelled via one single profile per state (i.e., 48 profiles per resource). For example, the solar PV capacity difference between the two set-ups exceeded 32 GW, or 10% of the total installed capacity for this technology. In a more recent assessment, Frysztacki et al. [22] evaluate the role of high-resolution RES siting in a study focusing on the European power system. They confirm the findings of [21] regarding the considerable impact of RES representation on the installed capacity requirements and, in addition, point out that modelling RES via 1024 different profiles leads to 10.5% lower system costs compared to more simplified set-ups using only 37 distinct profiles (i.e., one per country) per renewable resource. In the following, the detailed representation of RES to produce an accurate (i.e., high-resolution) assessment of the most suitable locations for asset deployment will be referred to as *siting*. A set-up where the detailed RES representation is integrated in models whose outcomes include installed capacities and associated costs, will be referred to as *sizing*.

The siting of RES assets has been a growing research topic lately. The models tackling this problem typically put more emphasis on the representation of renewable resources at the expense of other modelling features such as network or time-coupling constraints. In addition, they use non-monetary objectives such as, e.g., residual load or resource variability minimization. For instance, Jerez et al. [23] propose a tool which enables the distribution of RES capacities, as well as their output estimation via several transfer functions, across a regular grid with a spatial resolution of 0.44°. The problem is tackled by first computing distribution keys that take into account resource quality, population density and the existence of protected areas and then leveraging them to spread pre-defined capacities of RES across the system. Becker and Thrän [24] propose a method that sites wind generators such that the correlation (estimated via the Pearson coefficient) of the underlying resource with that of existing assets is minimized. A heuristic is also designed to solve the problem. Then, Musselman et al. [25] tackle the wind farm siting problem via two different bi-objective models formulated as mixed-integer linear programs (MILP). The first model seeks to simultaneously minimize (i) the average residual demand and (ii) the average power output variability (measured as the absolute change in residual demand between consecutive periods), while the second model simultaneously minimizes (i) the average residual demand and (ii) the maximum increase in residual demand over sets of time periods of pre-specified length. Furthermore, Hu et al. [26] use linear programming and portfolio optimization concepts to site RES assets such that the standard deviation of their aggregate feed-in (i.e., the

portfolio volatility) is minimized. However, overlooking the electricity demand in this process brings into question the ability of some of these methods [24,26] to achieve proper siting. A framework siting RES assets such that the occurrence of simultaneous, system-wide low-generation events is minimized has been recently proposed by Berger et al. [18]. The problem has since been cast as an integer program (IP) for which several solution methods have been proposed [27]. Although they offer a valuable overview of different siting criteria proposed in the literature, a common drawback of all these studies is that they fall short in evaluating the implications of the corresponding outcomes on the design and economics of power systems. Such a feature usually surfaces once a sizing model reveals the configuration of the power system.

The sizing of renewable power generation plants has been traditionally achieved via capacity expansion planning (CEP) frameworks, a class of problems which has received a great deal of attention in recent years [28]. For example, Baringo and Conejo [29] have studied the strategic investment in wind power generation assets by making use of a bi-level formulation in which investment decisions (siting and sizing) define the upper level and market clearing forms the lower level problem. In addition, Munoz et al. [30] tackled the joint generation and transmission expansion planning via a MILP where investment decisions are done in two stages, such that corrective actions are possible once uncertainty is revealed. In theory, such models are capable of evaluating the implications of RES siting on the design and economics of power systems. However, owing to computational limitations, these models usually have relatively low spatial and temporal resolutions, an aspect that makes it difficult to accurately capture correlations between variable renewable resources and properly site RES assets. Several attempts to integrate spatially-resolved siting of RES assets have been made, yet a common drawback can be identified across all of them. On the one hand, in line with [29,30] where purely economic criteria are optimized, a study by MacDonald et al. [15] leverages a CEP framework cast as a linear program (LP) to jointly optimize generation, transmission and storage capacities. The model is instantiated with hourly-sampled RES and demand data, while a 13 km regular grid is used for an accurate representation of renewable resources. However, the approach is reported to require thousands of core hours to solve large-scale instances, a feature which makes it difficult to reproduce and limits its use in practice. Another study making use of a cost-minimization CEP framework cast as an LP sites RES assets over a 0.75° regular grid [31]. This time, the formulation of the CEP problem relies on a highly simplified temporal representation of the renewable resource availability (i.e., the hourly resolution is replaced by a 144-step duration curve), an aspect that often limits the ability of the underlying model to accurately estimate system needs [32]. On the other hand, non-economic optimization criteria have also been used in sizing set-ups. For instance, Wu et al. [33] propose an IP for siting and sizing wind generation at high spatial resolutions (e.g., 3.6 km used in their study) such that the need for peak conventional generation feed-in is minimized. Nevertheless, their formulation, which relies on a full coefficient matrix, is computationally inefficient and its scalability is limited to a few hundred locations and one year of data with hourly resolution. In a similar fashion, Zappa and van den Broek [34] minimize year-round residual demand through a linearly constrained quadratic program. In the proposed model, RES assets are sited over the same regular grid used in [31]. However, their method suffers from similar scalability issues as [33], which limits the scale of problems tackled to a few hundred of RES sites and one year with hourly resolution.

In this paper, a method that enables the screening of thousands of candidate sites and tens of years of resources data is leveraged to evaluate the economic impact of different strategies for siting offshore wind across European Seas. To this end, a two-stage routine that bridges the gap between the streams of literature independently tackling the siting and sizing of RES assets in CEP frameworks is proposed. At first, siting of RES assets is addressed via an integer programming problem with a non-monetary objective. Then, linear programming is used to formulate a cost-minimization capacity expansion planning problem that unfolds some of the implications of siting RES assets according to predefined criteria.

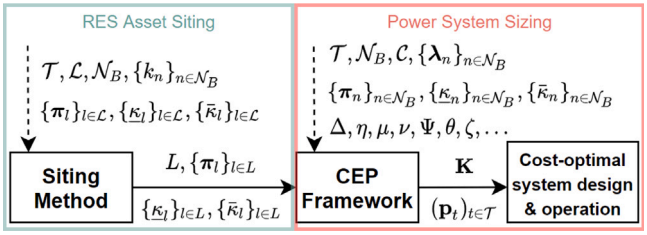

Fig. 1. Workflow of the proposed two-stage method. Dotted arrows denote exogenous input streams, while full arrows represent output streams, respectively.

3. Methodology

This section describes the two-stage method combining asset siting schemes and a capacity expansion planning model. Some basic notation used throughout this section is first introduced. The models and solution methods used in the siting stage are discussed next. Finally, the capacity expansion planning framework is presented. A visual representation of the proposed workflow is shown in Fig. 1.

3.1. Preliminaries

A finite time horizon $T \in \mathbb{N}$ and associated set of time periods $\mathcal{T} = \{1, \ldots, T\}$ are considered. A geographical area is represented by a finite set of sites $\mathcal{L}, |\mathcal{L}| = L$, which may be partitioned into a collection of disjoint regions $\mathcal{L}_n \subseteq \mathcal{L},\ \forall n \in \mathcal{N}_B$, where $\mathcal{N}_B$ with $|\mathcal{N}_B| = B$, may for instance represent the set of electrical buses in a power system and $\mathcal{L}_n$ may represent a set of candidate RES sites that may be connected to bus $n \in \mathcal{N}_B$. Each location $l \in \mathcal{L}$ is assumed to have a fixed technical potential $\bar{\kappa}_l \in \mathbb{R}_+$, which represents the maximum capacity that may be deployed at this location. In addition, some legacy capacity $\underline{\kappa}_l \in \mathbb{R}_+$ may have already been deployed at sites $l \in \mathcal{L}_0 \subseteq \mathcal{L}$. A time series $\mathbf{s}_l = (s_{l1}, \ldots, s_{lT}) \in \mathbb{R}_+^T$ describing renewable resource data (e.g., wind speed, solar irradiation) over $\mathcal{T}$ is assumed to be available at each location $l \in \mathcal{L}$. Furthermore, the instantaneous power output of location $l \in \mathcal{L}$ is estimated via a suitable transfer function h_l that returns per-unit capacity factor values $\pi_{lt} = h_l(s_{lt}), \forall t \in \mathcal{T}$, which are stored in a time series $\boldsymbol{\pi}_l = (\pi_{l1}, \ldots, \pi_{lT}) \in \{0, 1\}^T$. This transfer function may be that of a single RES power generation technology (e.g., a wind turbine or a solar PV module) or that of an entire power station (e.g., a wind farm or a PV power station).

3.2. Siting schemes

The models and solution methods used in asset siting schemes are described in this section.

3.2.1. Models

Models that select a pre-specified number of suitable candidate sites so as to optimize a given criterion are introduced. Two different criteria are considered, leading to two different siting schemes. The first criterion measures the aggregate power output ($PROD$), while the second one measures the spatiotemporal complementarity that sites exhibit ($COMP$). Both siting problems are cast as integer programming models.

Aggregate power output. This siting scheme selects a collection of disjoint subsets of locations so as to maximize their average capacity factor. More precisely, a pre-specified number of locations $k_n \in \mathbb{N}$ (including legacy locations) is selected in each region $\mathcal{L}_n$, and the total number of locations that must be deployed is $k = \sum_{n\in\mathcal{N}_B} k_n$. In order to formulate this problem as an IP, a set of binary variables is introduced. Indeed, a binary variable $x_l \in \{0,1\}$ is used to indicate whether location l is selected for deployment, that is, $x_l = 1$ if location l is selected for deployment and $x_l = 0$ otherwise. A binary matrix with entries $A_{nl} \in \{0,1\}$ is also used to indicate whether location l belongs to region $\mathcal{L}_n$, such that $A_{nl} = 1$ if this is the case and $A_{nl} = 0$ otherwise. Note that since regions are disjoint, each column of this matrix has exactly one nonzero entry, and we may assume without loss of generality that locations are ordered such that matrix A is block diagonal. The problem at hand then reads

$$\max_{x_l} \quad \frac{1}{k}\sum_{l\in\mathcal{L}} x_l\left[\frac{1}{T}\sum_{t\in\mathcal{T}}\pi_{lt}\right] \tag{1a}$$

$$\text{s.t.} \sum_{l\in\mathcal{L}} A_{nl}x_l = k_n,\ \forall n\in\mathcal{N}_B, \tag{1b}$$

$$x_l = 1,\ \forall l\in\mathcal{L}_0, \tag{1c}$$

$$x_l \in \{0,1\},\ \forall l\in\mathcal{L}. \tag{1d}$$

The objective function (1a) computes the average capacity factor of the locations selected for deployment. The cardinality constraints (1b) ensure that exactly k_n locations are selected in region $\mathcal{L}_n$, $\forall n \in \mathcal{N}_B$, while constraints (1c) guarantee that legacy assets are taken into account. Finally, constraints (1d) express the binary nature of location selection decisions.

Spatiotemporal complementarity. This siting scheme selects a collection of disjoint subsets of locations so as to maximize their spatiotemporal complementarity. Recall that, in this paper, locations are considered complementary if they rarely experience simultaneous low electricity production events (compared with a pre-specified reference production level) [18,27]. The framework that makes it possible to cast this problem as an IP is discussed next.

First, a set of time windows $\mathcal{W}$, $|\mathcal{W}| = W$, is constructed from the set of time periods $\mathcal{T}$. More precisely, a time window $\mathrm{w} \in \mathcal{W}$ can be seen as a subset $\mathcal{T}_\mathrm{w} \subseteq \mathcal{T}$ of δ successive time periods, and all time windows $\mathrm{w} \in \mathcal{W}$ have the same length δ. Note that successive time windows overlap and share exactly $\delta-1$ time periods, while the union of all time windows covers the set of time periods $\mathcal{T}$. Then, the per-unit power generation level $\bar{\pi}_{l\mathrm{w}} \in [0,1]$ of each candidate site $l \in \mathcal{L}$ is evaluated over the duration of each time window $\mathrm{w} \in \mathcal{W}$ using a prescribed measure g_l, such that $\bar{\pi}_{l\mathrm{w}} = g_l(\{\pi_{lt}\}_{t\in\mathcal{T}_\mathrm{w}})$. This measure may for instance compute the average production level over each window $\mathrm{w} \in \mathcal{W}$. This would essentially be equivalent to applying a moving average-based filter to the original power production signal and result in a smoothed power output signal. The degree of smoothing would be controlled by δ, which makes it possible to study resource complementarity on different time scales. A local, time-dependent reference production level $\alpha_{l\mathrm{w}} \in \mathbb{R}_+$ is also specified at each candidate site $l \in \mathcal{L}$, and may for instance be proportional to the electricity demand. A location $l \in \mathcal{L}$ is considered productive enough over window w if $\bar{\pi}_{l\mathrm{w}} \geq \alpha_{l\mathrm{w}}$. Location l is then said to *cover* window w and be *non-critical*. Checking whether this condition is satisfied for all locations and time windows enables the construction of a binary matrix with entries $D_{l\mathrm{w}} \in \{0,1\}$, such that $D_{l\mathrm{w}} = 1$ if location l covers window w and $D_{l\mathrm{w}} = 0$ otherwise. In order to formalize the intuitive definition of resource complementarity introduced earlier, a threshold $c \in \mathbb{N}$ is specified, such that for any subset of candidate locations $L \subseteq \mathcal{L}$, a window $\mathrm{w} \in \mathcal{W}$ is said to be *c-covered* or *non-critical* if at least c locations cover it (i.e., produce enough electricity over its duration). More formally, window w is non-critical if $\sum_{l\in L} D_{l\mathrm{w}} \geq c$.

Using the notation introduced for the first siting scheme, formulating the integer programming problem only requires the definition of a set of additional binary variables. More precisely, for each window $\mathrm{w} \in \mathcal{W}$, a binary variable $y_\mathrm{w} \in \{0,1\}$ indicating whether window w is non-critical is introduced, such that $y_\mathrm{w} = 1$ if window w is non-critical and $y_\mathrm{w} = 0$ otherwise. The problem of siting renewable power plants so as to maximize their spatiotemporal complementarity then reads

$$\max_{x_l, y_\mathrm{w}} \quad \sum_{\mathrm{w}\in\mathcal{W}} y_\mathrm{w} \tag{2a}$$

$$\text{s.t.} \sum_{l\in\mathcal{L}} D_{l\mathrm{w}}x_l \geq c y_\mathrm{w},\ \forall \mathrm{w}\in\mathcal{W}, \tag{2b}$$

$$\sum_{l\in\mathcal{L}} A_{nl}x_l = k_n,\ \forall n\in\mathcal{N}_B, \tag{2c}$$

$$x_l = 1,\ \forall l\in\mathcal{L}_0, \tag{2d}$$

$$x_l \in \{0,1\},\ \forall l\in\mathcal{L}, \tag{2e}$$

$$y_\mathrm{w} \in \{0,1\},\ \forall \mathrm{w}\in\mathcal{W}. \tag{2f}$$

The objective function (2a) simply computes the number of non-critical time windows observed over the time horizon of interest. Dividing the objective by the total number of time windows shows that it can be interpreted as quantifying the empirical probability of having sufficient levels of electricity production across at least c locations simultaneously. A low objective value therefore implies that simultaneous low electricity production events occur often, which indicates poor complementarity between locations. Constraints (2b) define the binary classification of time windows and express the fact that a time window $\mathrm{w} \in \mathcal{W}$ is non-critical if at least c locations selected for deployment cover it. The cardinality constraints (2c) ensure that exactly k_n locations are selected in region $\mathcal{L}_n$, $\forall n \in \mathcal{N}_B$, while constraints (1c) guarantee that legacy assets are accounted for in siting decisions. Finally, constraints (2e)–(2f) express the binary nature of location selection decisions and time window criticality, respectively.

3.2.2. Solution methods

The solution methods used to tackle problems (1) and (2) are discussed next.

Aggregate power output. Since the objective function (1a) is separable and the coefficient matrix in Eq. (1b) is block diagonal, problem (1a)–(1d) is straightforward to decompose and solve. More precisely, the k_n most productive locations can be selected independently in each region $\mathcal{L}_n$, $\forall n \in \mathcal{N}_B$. In each region $\mathcal{L}_n$, this can be achieved by successively (i) computing the average capacity factor of each location $\bar{\pi}_l = (1/T)\sum_{t\in\mathcal{T}}\pi_{lt}$, $\forall l \in \mathcal{L}_n$, (ii) sorting locations based on their average capacity factor $\bar{\pi}_l$, (iii) adding the locations with the highest average capacity factors to a set $L_n \subseteq \mathcal{L}_n$ that initially contains the legacy locations belonging to region n, until $|L_n| = k_n$. The solution L to problem (1) is then obtained by taking the union of these sets, $L = \bigcup_{n\in\mathcal{N}_B} L_n$.

Spatiotemporal complementarity. An approximate solution method relying on a mixed-integer relaxation (MIR) of problem (2) followed by a local search algorithm inspired by the simulated annealing algorithm [35] is used to tackle (2a)–(2f) [27]. The mixed-integer relaxation is formed by relaxing the integrality constraint (2f) of the time window variables. The key advantage of this approach lies in the fact that the siting variables $x_l, \forall l \in \mathcal{L}$, remain integer in the solution and subsets of locations $L_n \subseteq \mathcal{L}_n$, $\forall n \in \mathcal{N}_B$, can be directly extracted from them. The number of non-critical windows associated with this collection of subsets $L = \bigcup_{n\in\mathcal{N}_B} L_n$ can be computed via a function f_c such that

$$f_c(L) = \left|\left\{\mathrm{w}\in\mathcal{W}\,\middle|\,\sum_{l\in L} D_{\mathrm{w}l} \geq c\right\}\right|. \tag{3}$$

The local search algorithm starts from a subset of locations $L_0 \subseteq \mathcal{L}$ obtained by solving the mixed-integer relaxation of problem (2). Note that by construction, L_0 includes legacy locations and satisfies

Algorithm 1 Local Search Algorithm

Input $L_0,\ \mathcal{L}_0,\ \mathcal{N}_B,\ \{\mathcal{L}_n\}_{n\in\mathcal{N}_B},\ I,\ N,\ r,\ T,\ f_c$

$L \leftarrow L_0 \setminus \mathcal{L}_0$
for $n \in \mathcal{N}_B$ **do**
  $\mathcal{L}_n \leftarrow \mathcal{L}_n \setminus \mathcal{L}_0$
end for
$i \leftarrow 0$
while $i < I$ **do**
  $\tilde{\Delta} \leftarrow -\infty$
  $j \leftarrow 0$
  while $j < N$ **do**
    $\hat{L} \leftarrow L$
    $\mathbf{s} \leftarrow$ vector storing the number of sites to sample per region
    for $n \in \mathcal{N}_B$ **do**
      $S_+ \leftarrow \mathbf{s}(n)$ sites sampled from $\mathcal{L}_n \setminus L$ unif. at random
      $S_- \leftarrow \mathbf{s}(n)$ sites sampled from $\mathcal{L}_n \cap L$ unif. at random
      $\hat{L} \leftarrow (\hat{L} \setminus S_-) \cup S_+$
    end for
    $\hat{\Delta} \leftarrow f_c(\hat{L} \cup \mathcal{L}_0) - f_c(L \cup \mathcal{L}_0)$
    if $\hat{\Delta} > \tilde{\Delta}$ **then**
      $\tilde{L} \leftarrow \hat{L}$
      $\tilde{\Delta} \leftarrow \hat{\Delta}$
    end if
    $j \leftarrow j + 1$
  end while
  if $\tilde{\Delta} > 0$ **then**
    $L \leftarrow \tilde{L}$
  else
    $p \leftarrow \exp(\tilde{\Delta}/T(i))$
    draw b from Bernoulli distribution with parameter p
    if $b = 1$ **then**
      $L \leftarrow \tilde{L}$
    end if
  end if
  $i \leftarrow i + 1$
end while
$L \leftarrow L \cup \mathcal{L}_0$

Output $L, f_c(L)$

the cardinality constraints (2c). Since legacy locations cannot change, they are first removed from L_0 in order to initialize the incumbent solution $L \subseteq \mathcal{L}$. Likewise, legacy locations are removed from the set of candidate sites that may be selected in each region $\mathcal{L}_n,\ \forall n \in \mathcal{N}_B$. Then, the algorithm performs a fixed number of iterations $I \in \mathbb{N}$ in the hope of improving the incumbent solution. More specifically, in each iteration, a fixed number $N \in \mathbb{N}$ of neighbouring solutions is drawn at random from the neighbourhood of the incumbent solution. This neighbourhood is formed by solutions that satisfy the cardinality constraints (2c) and share exactly $k - r$ locations with the incumbent solution. A neighbouring solution $\hat{L}$ can be constructed from the incumbent solution as follows. For each region $\mathcal{L}_n$, $\mathbf{s}(n)$ different locations are sampled uniformly at random from both $\mathcal{L}_n \setminus L$ and $\mathcal{L}_n \cap L$, and these locations are swapped. The numbers of locations sampled in different regions are chosen at random such that the cardinality constraints (2c) remain satisfied and $\sum_{n\in\mathcal{N}_B} \mathbf{s}(n) = r$. Then, each of the N neighbouring solutions is tested against the incumbent solution and stored in a temporary candidate solution $\tilde{L}$ if it is found to outperform previously-explored neighbouring solutions. Their performance is evaluated via the difference $\tilde{\Delta}$ between the objectives achieved by the neighbouring and incumbent solutions. Once N neighbouring solutions have been explored, the candidate solution corresponds to a neighbouring solution that maximizes $\tilde{\Delta}$ among all sampled solutions. Note that $\tilde{\Delta}$ may be negative (i.e., if the algorithm does not manage to improve on the incumbent). If $\tilde{\Delta} > 0$, the candidate solution becomes the new incumbent solution. By contrast, if $\tilde{\Delta} < 0$, whether the candidate solution becomes the new incumbent solution depends on the outcome b of a random variable drawn from a Bernoulli distribution with parameter p. This parameter depends on both $\tilde{\Delta}$ and the so-called *annealing temperature* $T(i)$. Roughly speaking, the temperature controls the extent to which the search space is explored in an attempt to find better solutions and exit local optima. The temperature is specified by a *temperature schedule* that provides a temperature $T(i)$ for each iteration i. This procedure is repeated until the maximum number of iterations I is reached. Algorithm 1 summarizes these ideas.

3.3. Capacity expansion planning framework

Upon retrieving a suitable subset of locations $L \subseteq \mathcal{L}$ from the siting stage, the associated capacity factor time series $\{\boldsymbol{\pi}_l\}_{l\in L}$, legacy capacities $\{\underline{\kappa}_l\}_{l\in L}$ and technical potentials $\{\bar{\kappa}_l\}_{l\in L}$ are passed as input data to a capacity expansion planning (CEP) framework that determines the optimal power system design. More precisely, the CEP model described in (4a)–(4s) selects and sizes the power generation, transmission and storage assets that should be deployed and operated in order to satisfy pre-specified electricity demand levels across Europe at minimum cost subject to a set of technical and environmental constraints.

A set of working assumptions characterize the capacity expansion planning framework used in the current study. First, investment decisions in power system assets are made by a central planner that also operates the system, has perfect foresight, and whose goal is to minimize total system cost in a purely deterministic set-up. A static investment horizon is considered and the investment and operation problems are solved concurrently. Investment decisions are made once (at the beginning at the optimization horizon), while operational decisions are taken on an hourly basis. Second, investments in generation, transmission or storage capacities are continuous variables and transmission expansion is limited to the reinforcement of existing corridors. Third, the network is represented by (i) a set of existing nodes, which represent an aggregation of real electrical nodes and ii) a set of existing transmission corridors, which connect the aforementioned nodes. Legacy generation assets at existing nodes are taken into account. Additional dispatchable capacity (e.g., gas-fired power plants) may be added at those nodes, while additional RES generation capacity may also be built at existing nodes, provided that the local renewable potential is not fully exploited. Finally, as seen in (4a)–(4s), no unit commitment constraints are considered and the full operating range of dispatchable power plants is assumed stable.

$$\min_{\mathbf{K},(\mathbf{p}_t)_{t\in\mathcal{T}}} \quad \sum_{\substack{n\in\mathcal{N}_B\\ l\in L_n}} \left(\zeta^l + \theta^l_f\right) K_l + \sum_{\substack{n\in\mathcal{N}_B\\ j\in\mathcal{G}\cup\mathcal{R}\cup\mathcal{S}}} \left(\zeta^j + \theta^j_f\right) K_{nj} + \sum_{\substack{n\in\mathcal{N}_B\\ s\in S}} \zeta^s_S S_{ns} +$$
$$\sum_{c\in\mathcal{C}} \left(\zeta^c + \theta^c_f\right) K_c + \sum_{t\in\mathcal{T}} \omega_t \Big[\sum_{\substack{n\in\mathcal{N}_B\\ l\in L_n}} \theta^l_v p_{lt} + \sum_{\substack{n\in\mathcal{N}_B\\ g\in\mathcal{G}\cup\mathcal{R}}} \theta^g_v p_{ngt} +$$
$$\sum_{\substack{n\in\mathcal{N}_B\\ s\in S}} \theta^s_v (p^C_{nst} + p^D_{nst}) + \sum_{c\in\mathcal{C}} \theta^c_v |p_{ct}| + \sum_{n\in\mathcal{N}_B} \theta^{ens} p^{ens}_{nt} \Big] \tag{4a}$$

The objective (4a) includes the capacity-dependent investment and fixed operation and maintenance (O&M) costs and the output-dependent variable O&M expenditures. In addition, an economic penalty is enforced on electricity demand shedding. Then, the electricity supply and demand balance is enforced via (4b).

$$\text{s.t.} \sum_{\substack{n\in\mathcal{N}_B\\ l\in L_n}} p_{lt} + \sum_{g\in\mathcal{G}\cup\mathcal{R}} p_{ngt} + \sum_{s\in S} p^D_{nst} + \sum_{c\in C^+_n} p_{ct} + p^{ens}_{nt}$$
$$= \lambda_{nt} + \sum_{s\in S} p^C_{nst} + \sum_{c\in C^-_n} p_{ct},\ \forall n \in \mathcal{N}_B, \forall t \in \mathcal{T} \tag{4b}$$

The operation and deployment of the RES units whose locations are determined by leveraging the siting models in Section 3.2 are constrained by (4c) and (4d), respectively. The next six equations model the

operation and sizing of the remaining generation units, including RES technologies that are not sited. More specifically, modelling aspects such as instantaneous feed-in (4e), ramp rates (4f)–(4g), minimum operating levels (4h), CO_2 emission levels (4i) or technical potential limitations (4j) are considered.

$$p_{lt} \leq \pi_{lt}(\underline{\kappa}_l + K_l),\ \forall l \in L_n, \forall n \in \mathcal{N}_B, \forall t \in \mathcal{T} \tag{4c}$$

$$\underline{\kappa}_l + K_l \leq \bar{\kappa}_l,\ \forall l \in L_n, \forall n \in \mathcal{N}_B \tag{4d}$$

$$p_{ngt} \leq \pi_{nt}(\underline{\kappa}_{ng} + K_{ng}),\ \forall n \in \mathcal{N}_B, \forall g \in \mathcal{G}, \forall t \in \mathcal{T} \tag{4e}$$

$$p_{ngt} - p_{ngt-1} \leq \Delta_g^+(\underline{\kappa}_{ng} + K_{ng}),\ \forall n \in \mathcal{N}_B, \forall g \in \mathcal{G}, \forall t \in \mathcal{T} \setminus \{0\} \tag{4f}$$

$$p_{ngt} - p_{ngt-1} \geq -\Delta_g^-(\underline{\kappa}_{ng} + K_{ng}),\ \forall n \in \mathcal{N}_B, \forall g \in \mathcal{G}, \forall t \in \mathcal{T} \setminus \{0\} \tag{4g}$$

$$\mu_g(\underline{\kappa}_{ng} + K_{ng}) \leq p_{ngt},\ \forall n \in \mathcal{N}_B, \forall g \in \mathcal{G}, \forall t \in \mathcal{T} \tag{4h}$$

$$q_{ngt}^{CO_2} = \nu_g^{CO_2} p_{ngt}/\eta_g,\ \forall n \in \mathcal{N}_B, \forall g \in \mathcal{G}, \forall t \in \mathcal{T} \tag{4i}$$

$$\underline{\kappa}_{ng} + K_{ng} \leq \bar{\kappa}_{ng},\ \forall n \in \mathcal{N}_B, \forall g \in \mathcal{G} \tag{4j}$$

It is worth mentioning the two most common situations in which the latter six constraints are enforced. On the one hand, if dispatchable units are modelled (e.g., gas-fired power plants), the time-dependent availability π_{nt} in Eq. (4e) is set to one across the entire optimization horizon. On the other hand, if a RES technology not sited via the models in Section 3.2 is addressed, the aforementioned parameter is instantiated with a per-unit capacity factor time series that is aggregated at the spatial resolution represented by bus $n \in \mathcal{N}_B$. Furthermore, the per-unit ramp rates Δ_g^+ and Δ_g^- in Eq. (4f)–(4g) are set to one, while the must-run and the specific CO_2 emission levels μ_g and $\nu_g^{CO_2}$, respectively, are set to zero.

$$p_{nst}^D \leq K_{ns},\ \forall n \in \mathcal{N}_B, \forall s \in S, \forall t \in \mathcal{T} \tag{4k}$$

$$p_{nst}^C \leq \phi_s K_{ns},\ \forall n \in \mathcal{N}_B, \forall s \in S, \forall t \in \mathcal{T} \tag{4l}$$

$$e_{nst} = \eta_s^{SD} e_{nst-1} + \omega_s \eta_s^C p_{nst}^C - \omega_s \frac{1}{\eta_s^D} p_{nst}^D,\ \forall n \in \mathcal{N}_B, \forall s \in S, \forall t \in \mathcal{T} \tag{4m}$$

$$\mu_s S_{ns} \leq e_{nst} \leq S_{ns}, \forall n \in \mathcal{N}_B, \forall s \in S, \forall t \in \mathcal{T} \tag{4n}$$

$$\underline{\kappa}_{ns} \leq S_{ns} \leq \bar{\kappa}_{ns},\ \forall n \in \mathcal{N}_B, \forall s \in S \tag{4o}$$

Storage units are modelled via (4k) to (4o), assuming independent energy and power ratings and asymmetric charge and discharge rates, while constraints (4p) and (4q) define the transportation model governing the flow in transmission assets.

$$|p_{ct}| \leq (\underline{\kappa}_c + K_c),\ \forall c \in C, \forall t \in \mathcal{T} \tag{4p}$$

$$\underline{\kappa}_c + K_c \leq \bar{\kappa}_c,\ \forall c \in C \tag{4q}$$

$$\sum_{\substack{n \in \mathcal{N}_B \\ g \in \mathcal{G} \\ t \in \mathcal{T}}} q_{ngt}^{CO_2} \leq \Psi^{CO_2} \tag{4r}$$

$$\sum_{d \in \mathcal{D}} K_{nd} + \sum_{r \in \mathcal{R}} \Pi_{nr} K_{nr} + \sum_{l \in L_n} \Pi_l K_l \geq (1 + \Phi_n)\hat{\lambda}_n,\ \forall n \in \mathcal{N}_B \tag{4s}$$

A system-wide CO_2 budget is enforced via (4r). Then, a system adequacy constraint is enforced via (4s) following the definition provided in [36], according to which a system is adequate in the long-term by ensuring that the amount of firm capacity exceeds the peak demand by a planning reserve margin. According to Eq. (4s), this constraint is enforced at every bus $n \in \mathcal{N}_B$ and the corresponding peak demands and reserve margins are defined by $\hat{\lambda}_n$ and Φ_n, respectively. There are two main sources providing firm capacity. On the one hand, set $\mathcal{D}$ in the first term on the left-hand side gathers dispatchable power generation technologies. On the other hand, RES assets also contribute to the provision of firm capacity and their participation is proportional to their capacity credit, as defined in [37]. To this end, two sets of RES technologies are defined. The one in the second term of (4s) gathers the subset of RES technologies which are not sited, while L_n defines, for every $n \in \mathcal{N}_B$ the collection of sites obtained from the previous siting stage.

3.4. Implementation

With the exception of the siting algorithm (detailed in Section 3.2.2) which was implemented in Julia 1.4, the implementation of the proposed framework is based on Python 3.7. All simulations were run on a workstation running under CentOS, with an 18-core Intel Xeon Gold 6140 CPU clocking at 2.3 GHz and 256 GB RAM. The sizing problem (4a)–(4s) is implemented in PyPSA 0.17 [38]. Gurobi 9.1 was used to solve the MIR of (2a)–(2f), as well as (4a)–(4s).

4. Case study

The upcoming section describes the case study used to investigate (i) the outcome of siting offshore wind plants within European borders by leveraging the two siting strategies introduced in Section 3.2 and (ii) the impact these siting strategies have on the resulting power system configurations. First, the realistic set-up used in the siting stage is presented. Then, the main features of the CEP framework are introduced. Recall that, in this exercise, offshore wind is the only renewable resource for which siting decisions are analysed, while the other RES technologies (i.e., onshore wind, utility-scale and distributed PV) are modelled via aggregate, per-country profiles obtained from the *renewables.ninja* data platform [39,40].

4.1. Offshore wind siting

Renewable resource data. For this analysis, ten years (i.e., 2010 to 2019) of hourly-sampled wind speed data at a spatial resolution of 0.25° are obtained from the ERA5 reanalysis dataset [19]. The time series are then re-sampled by preserving the mean of each consecutive subset of three hours across the entire time horizon, yielding $T = 29216$ time periods. The conversion of raw resource data into capacity factor time series (a step required in both siting strategies introduced in Section 3.2) is achieved by applying the transfer function of a wind farm to the time series of wind speeds. Determining the appropriate wind farm transfer function for each candidate site involves a two-step process. First, the ten-year average wind speed is computed and the relevant IEC wind class is determined [41]. Once the wind class is known, an appropriate wind turbine is selected (in this exercise, two wind turbines are available, i.e., the Vestas V90 and V164 models) and the corresponding farm-specific transfer function is determined via a power curve smoothing procedure inspired from [42].

Deployment targets. In order to compute the number of sites k that should be considered for deployment, the siting stage assumes the need for up to 450 GW of offshore wind across 19 European Exclusive Economic Zones (EEZ), in line with a recent study published under the aegis of the European Commission [7]. Mapping this capacity to a number of sites required to host it yields a total of $k = 353$ sites throughout European Seas, among which 135 are locations with existing capacity at the time of the planning exercise. The per-country distribution of sites, as well as the details leading to this estimation are gathered in the Supplementary Material. It is worth mentioning that throughout the analysis, both partitioned (i.e., $B = 19$, where offshore wind sites are deployed whilst respecting the territorial boundaries of the 19 countries considered in this study) and unpartitioned (i.e, $B = 1$, where the $k = \sum_{n \in \mathcal{N}_B} k_n$ sites are freely deployed across European Seas) siting strategies will be investigated.

COMP siting set-up. The $COMP$ siting strategy is carried out for a time window length δ of one time period (i.e., three hours). Then, a location $l \in \mathcal{L}$ is considered non-critical during time window w if its maximum theoretical generation potential exceeds a pre-defined share of the system-wide electricity demand. By expressing the former as the product between the technical potential $\bar{\kappa}_l$ and the capacity factor $\bar{\pi}_{l\mathrm{w}}$, this condition can be written as

$$\bar{\kappa}_l \bar{\pi}_{l\mathrm{w}} \geq \frac{\varsigma \bar{\lambda}_{\mathrm{w}}}{k}\ , \tag{5}$$

where ς represents the proportion of the electricity demand during window w (i.e, $\bar{\lambda}_w$) to be covered by offshore wind plants (which in this exercise is uniformly set to 30%, as suggested in [43]) and k denotes the number of system-wide offshore wind deployments. Dividing both sides of Eq. (5) by $\bar{\kappa}_l$ yields the local criticality definition introduced in Section 3.2.1, with the reference production level $\alpha_{lw} = \varsigma\bar{\lambda}_w/\bar{\kappa}_l k$. Furthermore, threshold c in Eq. (2b) is set such that at least half of the locations must cover any time window for it to be labelled non-critical. In order to retrieve the $COMP$ set of sites, Algorithm 1 is run thirty times and the solution with the highest objective function (i.e., the highest number of non-critical windows) is retrieved and passed to the subsequent CEP stage. With respect to the algorithm parameters, a neighbourhood radius r of 1, an initial temperature T of 100 and an exponential temperature schedule $T(i) = 100 \times \exp(-10 \times i/I)$ were considered. Additionally, $I = 5000$ iterations with $N = 500$ neighbouring solutions each are considered for each run of the algorithm. The resulting instance contains 31688 integer variables and is solved, on average, in 6300 s on the machine described in Section 3.4.

4.2. Capacity expansion problem

Network topology. The set of countries considered in the sizing stage includes, aside from the 19 countries listed in Table 1 of the Supplementary Material, Austria, Hungary, Czechia, Slovakia, Switzerland (as landlocked territories), Bulgaria, Romania and Slovenia (with no offshore wind capacity mentioned in [7]). It should be noted that $L_n = \emptyset$ for the subset of countries previously mentioned (i.e., no offshore wind sites available). Each country is modelled as one node, while the network topology is based upon that used for the 2018 version of the European TYNDP [44]. A map of the topology is provided in the Supplementary Material. It is hereby assumed that all interconnections crossing bodies of water are developed as DC cables, while the remainder are AC cables. As mentioned previously, transmission expansion decisions are limited to the reinforcement of existing corridors. The connection costs of offshore sites to the associated onshore buses depend on the capacity of the generation unit (representing a 20% share of the capital expenditure [45]), but not on the distance to shore. Hourly-sampled demand data covering the same ten years used in the siting stage (i.e., 2010 to 2019) is retrieved from [46]. Then, as in the previous siting stage, time series are resampled at three-hourly resolution by preserving the mean of each consecutive subset of three hours across the entire time horizon.

Electricity generation assets. There are nine technologies available for electricity generation, i.e., offshore and onshore wind, utility-scale and distributed solar PV, run-of-river and reservoir-based hydro, nuclear plants, open- and combined-cycle gas turbines (OCGT and CCGT, respectively). Only a subset of these technologies (i.e., the offshore wind and the gas-fired units) are sized, while installed capacities of onshore wind, solar PV, hydro and nuclear power plants remain fixed throughout the optimization. Recall that the technical potentials of the offshore wind sites are inputs from the siting stage. By contrast, those of the remaining generation technologies to be sized in the CEP framework (i.e., OCGT and CCGT) are assumed to be unconstrained. All generation technologies except the gas-fired power plants are assumed to have non-zero installed capacities at the beginning of the optimization exercise. More specifically, 61.5 GW of nuclear power capacity, 33.5 GW of run-of-river hydro power capacity and 98.1 GW of reservoir-based hydro power capacity are available throughout the selected European countries [47,48][1]. Existing wind capacity is obtained from [49], where 99.1 GW of offshore wind and 160.5 GW of onshore wind capacity in various development stages are reported across Europe. Utility-scale solar PV capacity data is retrieved from [50], where a legacy capacity of 45.5 GW is reported throughout Europe. Finally, country-aggregated capacities for distributed PV installations are retrieved from [51], where the existence of 77.7 GW of such installations is reported within European borders.

Electricity storage assets. Two technologies are available for storing electricity, namely, pumped-hydro (PHS) and battery storage (Li-Ion). It is assumed that no legacy capacity is available in Europe for the latter. Pumped-hydro units are not sized within the CEP framework at hand and the power ratings of existing plants are retrieved from [48], where a total of 54.5 GW/1950 GWh of PHS units are reported[2]. A summary of the techno-economic data used to instantiate the CEP problem is provided in Table 1.

Policy constraints. A set of policy-related constraints are enforced in the CEP problem. One of the main constraints driving the design of power systems under deep decarbonization targets is the CO_2 budget. In the current exercise, this budget is enforced system-wide and its value imposes a 90% reduction in carbon dioxide emissions throughout the optimization horizon relative to 1990 levels. Then, a planning reserve margin of 20% is considered at each bus $n \in \mathcal{N}_B$ via Eq. (4s). The set D gathering dispatchable generation units providing firm capacity includes OCGT, CCGT, nuclear and reservoir-based hydro power plants. Furthermore, at each bus $n \in \mathcal{N}_B$, the capacity credit of RES sites is computed during the top 5% time instants of peak electricity demand.

All these yield a model with 57×10^6 variables and 26.8×10^6 constraints, which solves in just over 25 h on the machine described in Section 3.4. A detailed account of the techno-economic assumptions considered in this study is provided in the Supplementary Material. The input data used to set-up the siting and sizing models is available at [52]. The code used to run both models is available at [16] and [17], respectively.

5. Results

In this section, a series of experiments that compare the implications of the proposed siting schemes on the design and economics of power systems is conducted. In particular, the impact of two variants (i.e., partitioned and unpartitioned) of $PROD$ and $COMP$ on the siting of roughly 350 offshore wind power plants in the European power system is discussed.

5.1. Impact of siting decisions on offshore production and residual load

The first set of results provides insight into the impact of the two siting strategies on the aggregate offshore wind and residual demand signals. To this end, an unpartitioned set-up is used (i.e., where sites are deployed with no consideration for territorial constraints), whose outcome can be seen in Fig. 2 for both $PROD$ and $COMP$ schemes, where green markers depict the 135 legacy offshore wind sites common across the two strategies. On the left, the $PROD$ strategy concentrates all remaining sites to be deployed in two of the most productive areas in the European Seas (i.e., the Atlantic region offshore the British Isles and the North Sea area between Denmark and Norway) [5]. By contrast, the right-hand side subplot shows that the $COMP$ strategy distributes sites across several distinct areas found within European EEZs. More specifically, offshore wind deployments under this strategy seem to follow two directions. On the one hand, resource-rich sites in the Atlantic region are still exploited, though to a lesser extent considering that the very good resource in the North Sea basin is already well represented in the set of legacy sites. On the other hand, a significant share of the sites picked by $COMP$ are spread in two regions

[1] The modelling of run-of-river capacity factors and of inflows into the water storage of reservoir-based hydro plants is detailed in the Supplementary Material.

[2] The specific durations of these units is estimated on a unit-by-unit basis via a procedure that is detailed in the Supplementary Material.

Table 1
Summary of techno-economic parameters used to instantiate the CEP problem. N/A values denote either (i) the lack of a capacity upper bound or (ii) economic information which is irrelevant for the purpose of this study. Data sources are provided in the Supplementary Material.

Technology	$\underline{\kappa}$ GW(h)	$\bar{\kappa}$ GW(h)	CAPEX M€/GW(h)	FOM M€/GW(h)-yr	VOM M€/GWh	Lifetime yrs
Onshore Wind	160.51	160.51	N/A	29.47	0.00	N/A
Offshore Wind	99.14	≈450.00[a]	1881.08	49.11	0.00	25
Utility-Scale PV	45.52	45.52	N/A	7.14	0.00	N/A
Distributed PV	77.69	77.69	N/A	5.36	0.00	N/A
OCGT	0.0	N/A	838.87	3.03	0.0076	30
CCGT	0.0	N/A	1005.27	7.58	0.0053	30
Nuclear	61.55	61.55	N/A	106.25	0.0018	N/A
Run-of-River Hydro	33.52	33.52	N/A	0.00	0.0119	N/A
Reservoir Hydro	98.12	98.12	N/A	0.00	0.0152	N/A
Pumped-Hydro	54.54	54.54	N/A	14.20	0.0002	N/A
Battery Storage[b]	0.00	N/A	100.00 / 94.00	0.54	0.0017	10
HVAC	100.61	N/A	2.22	0.017	0.00	40
HVDC	31.07	N/A	1.76	0.021	0.00	40

[a]Value to be interpreted as a lower bound on the real value which depends on the outcome of the sizing stage (as the potential of each site is proportional to its corresponding surface area which, in turn, depends on the latitude).
[b]For battery storage (Li-ion), the values before and after the slash sign under the CAPEX header express the capital expenses for power and energy components. Moreover, the FOM is expressed in M€/GW and applies to the power component, while the VOM is expressed in M€/GWh and applies to the energy component.

(i.e., Iberia and Southeastern Europe) that are known to have distinct and complementary wind regimes to the ones in Northern Europe, as pointed out in [53,54].

The effects of offshore wind power plant siting decisions on the aggregate offshore wind and residual load signals can be seen in Figs. 3 and 4. More specifically, Fig. 3 displays the aggregate offshore wind signal (top subplot) as well as the aggregate residual demand signal (bottom subplot). The signal shown in the top subplot is obtained by spatially averaging the capacity factor time series of the 353 locations selected by the two siting schemes under consideration, while the aggregate residual demand signal is calculated as follows: (i) the technology power density and site area assumptions considered in the Supplementary Material for the estimation of the deployment targets are preserved and (ii) the demand signals of the European countries considered in the sizing stage (i.e., the 19 countries with offshore wind deployments and the eight additional ones with no such targets) are summed to yield a single Europe-wide profile from which the aggregate offshore wind feed-in is subtracted. Fig. 4, on the other hand, shows the statistical distribution of the residual demand (4a) as well as the statistical distribution of the spread between the maximum and minimum residual demand for 12-hourly and daily (disjoint) time periods (4b and 4c). All distributions are constructed using data from ten weather years (2010–2019).

Fig. 3 suggests that the $COMP$ scheme is indeed able to select sites with fewer periods of simultaneous low electricity production than the $PROD$ one. More precisely, aggregate capacity factor values stay between (roughly) 30% and 60% for the $COMP$ scheme while the range of capacity factor values covered by the $PROD$ scheme is much broader. This observation is consistent with the fact that the $COMP$ deployment pattern covers 29031 time windows (out of 29218), while the $PROD$ pattern covers 27147 time windows (around 6.5% fewer than $COMP$), which also implies that instances of high residual load are more frequent in the $PROD$ pattern. This claim is supported by Fig. 4a, which shows that the $COMP$ scheme leads to an overall reduction in residual demand. Indeed, the first quartile, the median, the third quartile and the maximum of the $COMP$ scheme all correspond to significantly lower residual demand values than those of the $PROD$ scheme. Furthermore, Fig. 3 suggests that some degree of aggregate output variability reduction on time scales ranging from hours to days may be obtained as a by-product of the $COMP$ scheme. This intuition is also supported by the box plots in Figs. 4b and 4c, which indicate that both the full and interquartile ranges of siting patterns produced by the $COMP$ scheme are narrower than those obtained by the $PROD$ scheme. Finally, in Fig. 3c, it can be seen that the $COMP$ scheme sometimes produces less than $PROD$ for a few days in a row, which can partly be attributed to the fact that the $PROD$ scheme maximizes the average capacity factor.

Variants of the $PROD$ and $COMP$ siting schemes that select locations while satisfying country-based deployment targets ($B = 19$, as shown in Table 1 of the Supplementary Material) are analysed next. The

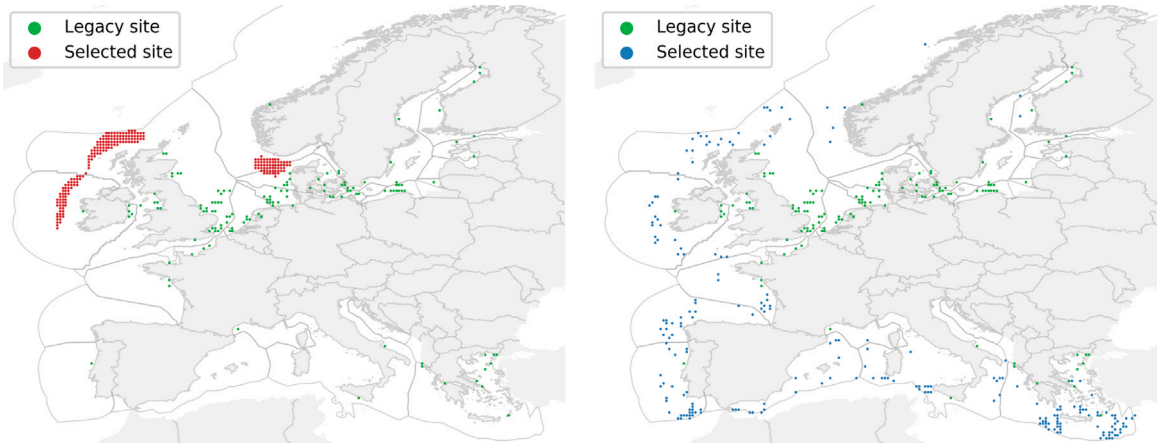

Fig. 2. Deployment patterns for the $PROD$ (left) and $COMP$ (right) siting schemes for the unpartitioned ($B = 1$) case. In both plots, legacy locations are displayed in green. Exclusive Economic Areas depicted by the grey contours outside the European land mass.

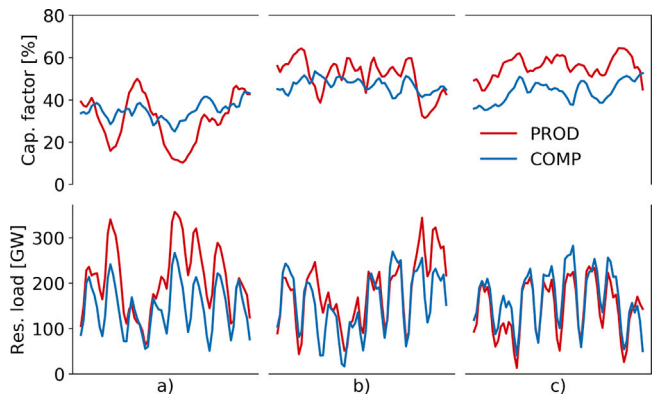

Fig. 3. Visual examples of aggregate offshore wind (top) and residual demand (bottom) signals for the unpartitioned ($B = 1$) $PROD$ and $COMP$ schemes.

associated $PROD$ and $COMP$ deployment patterns are shown in Fig. 5, where green markers depict legacy locations. In this context, the $PROD$ scheme (left) yields a set of clusters of locations, which correspond to the most productive areas of each EEZ. Hence, the resulting deployment pattern is much more scattered than the one observed in the unpartitioned set-up and benefits from much more diverse wind regimes, as suggested by Grams et al. [53]. The $COMP$ pattern (right) is even more scattered than the $PROD$ one. Legacy locations are common to both schemes and about 19% of non-legacy locations selected by the $COMP$ scheme are also selected by the $PROD$ scheme, up from 6% in the unpartitioned set-up. The partitioned $PROD$ and $COMP$ patterns therefore share a total of 176 locations (i.e., roughly 50% of all selected locations). Furthermore, in several countries, the number of candidate locations available is only slightly greater than the number of locations that must be deployed there. Hence, even though locations selected in these countries by the $PROD$ and $COMP$ schemes may not be exactly identical, they nevertheless end up being in the direct vicinity of one another and therefore experience very similar wind regimes. This is especially true in the Baltic Sea and in countries like Denmark or the Netherlands. This also happens in countries such as France and Ireland, though to a lesser extent, in spite of the fact that the numbers of candidate locations available far exceed the numbers of locations that must be deployed there.

Overall, this analysis suggests that the two siting schemes are likely to yield deployment patterns whose performance are comparable. Inspecting the $COMP$ siting objectives achieved by both deployment patterns confirms this intuition. More precisely, the $COMP$ pattern covers 27981 windows, while the $PROD$ pattern covers 27688 windows. In other words, there is only a 1% difference between them. In addition, Fig. 6 shows the distributions of residual demand aggregated across Europe and on a country-by-country basis. At the notable exception of Norway, where the median residual load of the $COMP$ scheme is slightly higher than that of the $PROD$ scheme, the residual demand distributions that both schemes yield are virtually identical. Interestingly, the first quartile, median and third quartile of the Europe-wide $COMP$ distribution correspond to residual demand levels that are slightly higher than those observed for the $PROD$ distribution, while maximum residual levels are virtually identical for both schemes. Hence, these results suggest that enforcing country-based deployment targets and selecting locations in the most productive areas is enough to take advantage of the diversity that exists in European offshore wind regimes.

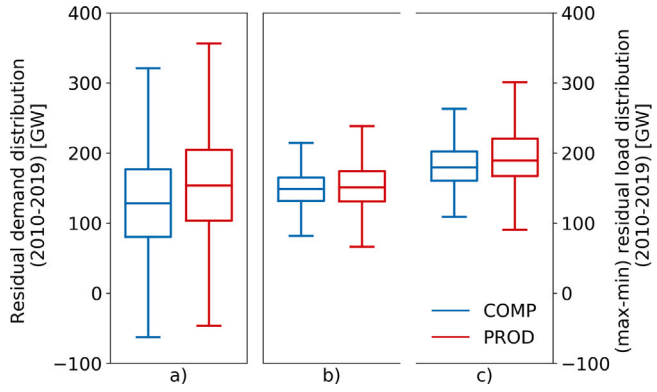

Fig. 4. Statistical distribution of the residual demand under the unpartitioned ($B = 1$) $PROD$ and $COMP$ siting schemes (left). Statistical distribution of the (max–min) spread for 12-hourly and daily disjoint intervals of the residual demand time series under the unpartitioned ($B = 1$) $PROD$ and $COMP$ siting schemes (right). Boxes depict the first quartile, median and third quartile of time series, respectively.

5.2. Impact of siting decisions on capacity expansion planning outcomes

In this section, the impact of different siting schemes on the outcomes of the capacity expansion planning set-up described in Section 3.3 are investigated. To this end, the outcomes of the two variants of the two siting schemes introduced in Section 3.2 (four in total, i.e., $B = 1$ vs $B = 19$ for both $PROD$ and $COMP$) are used to run the CEP stage over the ten individual weather years included in the siting optimization problem (i.e., 2010 to 2019).

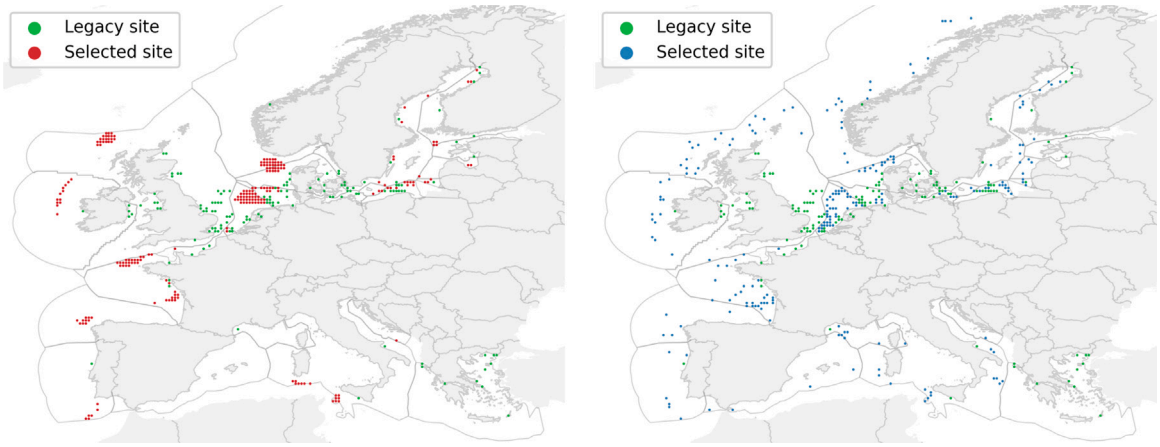

Fig. 5. Deployment patterns for the $PROD$ (left) and $COMP$ (right) siting schemes for the unpartitioned ($B = 19$) case. In both plots, legacy locations are displayed in green. Exclusive Economic Areas depicted by the grey contours outside the European land mass.

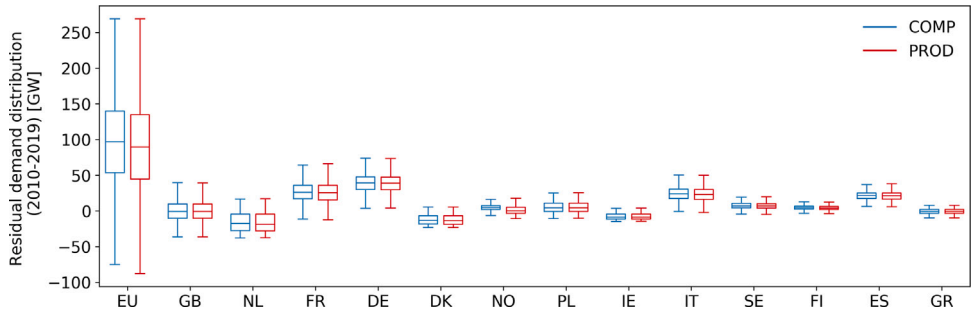

Fig. 6. Statistical distributions of residual demand time series (i) aggregated across Europe and (ii) in countries with more than $k_n = 10$ deployments under the partitioned ($B = 19$) $PROD$ and $COMP$ siting schemes.

5.2.1. Impact on power system economics

Fig. 7 gathers the objectives (i.e., annualized system costs) achieved in the forty aforementioned runs. First, the scatter plot shows distinct trends across partitioned and unpartitioned siting schemes, respectively. On the one hand, $COMP$ seems to outperform $PROD$ consistently (i.e., by 0.4% to 5.9% depending on the weather year considered) across the ten weather years when partitioning constraints are not enforced ($B = 1$). By contrast, when country-based deployment targets ($B = 19$) are accounted for in the siting of offshore wind power plants, the $PROD$ scheme leads to annualized system costs that are between 1.2% and 2.8% lower than those achieved by the $COMP$ scheme, depending on the weather year considered. In addition, this plot shows a great deal of variability in the sizing objectives achieved by different siting schemes and for different weather years (e.g., differences of up to 20% between the partitioned and unpartitioned $PROD$ schemes). This suggests that both siting decisions and inter-annual weather variability can have a substantial impact on the economics of power systems relying heavily on weather-dependent renewable generation assets such as offshore wind power plants. Unless otherwise stated, the analyses carried out in the next sections focus on the two extreme weather years (i.e., 2010 and 2014) in order to gain a better understanding of how siting decisions affect power system design.

5.2.2. Impact on power system design

A summary of relevant system design indicators is provided in Table 2, where the CEP outcomes of eight different runs (i.e., two weather years, two siting strategies, two deployment set-ups) are reported.

The first half of Table 2 gathers results obtained for CEP instances constructed using unpartitioned deployment patterns ($B = 1$, depicted in Fig. 2). A number of observations can be made. First, higher offshore wind capacities are observed in $COMP$-based configurations. This is due to the fact that the average capacity factors (41.5% and 41.6% for 2010 and 2014, respectively) are lower than the ones of the set of sites corresponding to $PROD$ (43.0% and 45.0% for 2010 and 2014, respectively), an aspect which inherently leads to higher installed capacities in the former scheme (considering that both $PROD$ and $COMP$ are required to meet the same electricity demand profile). More installed capacity leads to more electricity generation from these units in the 2010 instance and also to a significant reduction in curtailment volumes in both weather years considered. Moreover, maybe the most notable effect of deploying sites based on $COMP$ is a reduction in dispatchable capacity requirements. Recall that $COMP$ is designed to minimize the occurrence of system-wide resource scarcity events, such as the one depicted in Fig. 3a. As a result, the corresponding sizing instances consistently reveal smaller capacities for dispatchable generation units. More specifically, OCGT and CCGT capacities are reduced by up to 18.2% and 49.8% compared to the corresponding $PROD$ runs. This also translates into considerably smaller generation volumes from these units, with the exception of OCGT in the 2014 run, where the additional 2.4 TWh are used to replace the generation deficit brought up by offshore wind. Furthermore, Li-Ion does not seem to play a significant role in the design of the resulting systems (an aspect that holds across all subsequent runs). This outcome has two main causes. First, considerable pumped-hydro storage capabilities exist as legacy installations in the system under study. Second, the time resolution used in this exercise (i.e., three-hourly) does not capture short-term balancing events for which Li-Ion storage is particularly appealing. With respect to transmission capacities, it appears that $COMP$ is on par with $PROD$ in the 2010 instance (though a 15.7% increase in flows leads to a more efficient utilization of the infrastructure), while a reduction of 16.4% is observed in the 2014 run. Put together, these outcomes lead to total system cost reductions under the $COMP$ scheme of 5.9% (for 2010) and 3.6% (for 2014). It is worth pointing out that cost savings achieved by a reduction in dispatchable capacity deployment and use are partly offset by an increase in offshore wind capacity deployment, which is comparatively much more expensive per unit capacity.

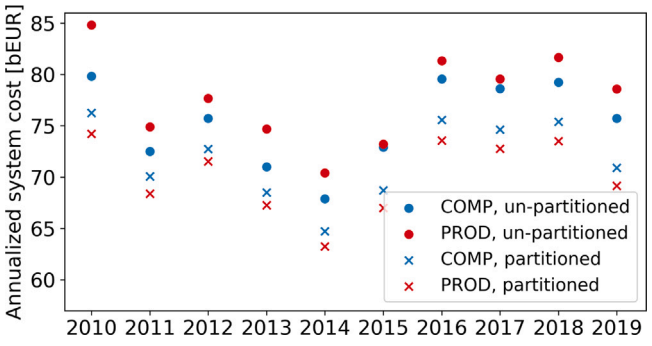

Fig. 7. Capacity expansion objectives of single-year set-ups instantiated with the outcomes of partitioned ($B = 19$) and unpartitioned ($B = 1$) $PROD$ and $COMP$ siting schemes.

Results pertaining to CEP instances constructed from partitioned deployment patterns ($B = 19$, shown in Fig. 5) are provided in the second half of Table 2. To begin with, the number of non-critical windows obtained for these set-ups reveal a much smaller difference between the two deployment schemes, i.e., 94.71% (or 27688) and 95.77% (or 27981) for $PROD$ and $COMP$, respectively. In terms of system costs, partitioned $PROD$ regularly out-performs partitioned $COMP$, as already shown in Fig. 7. Specifically, the latter scheme leads to system configurations which are 2.8% (for the 2010 instance) and 2.3% (for the 2014 case) more expensive than the corresponding $PROD$-based runs. This outcome can be explained as follows. Regardless of the weather year considered, the $COMP$-based runs deploy more offshore wind capacity (an additional 3.1% and 2.9% in the 2010 and 2014 runs, respectively), which translates into higher capital expenditures. Nevertheless, the associated generation levels are slightly inferior to those of the $PROD$-specific instances due to the differences between the capacity factors of the sets of sites associated with the two siting

Table 2
Comparison of annualized system costs and installed capacities for various technologies sized in the CEP framework. The analysis is conducted for the partitioned ($B = 1$) and unpartitioned ($B = 19$) variants of the $PROD$ and $COMP$ siting schemes and for a weather year with inferior (i.e., 2010) and superior (i.e., 2014) wind quality, respectively.

	Weather year	2010				2014			
	Siting scheme	$PROD$		$COMP$		$PROD$		$COMP$	
	Indicator	K[a]	p[b]	K	p	K	p	K	p
unpartitioned ($B = 1$)	W_{off}[c]	416.4	1532.4 (29.7)	463.8	1679.2 (25.4)	397.0	1517.9 (41.3)	411.3	1514.1 (15.7)
	OCGT	298.6	5.3	286.2	4.7	308.6	7.1	252.4	9.5
	CCGT	73.7	179.2	36.9	56.8	25.0	24.7	20.3	21.4
	Li-Ion	0.01	N/A	0.01	N/A	0.01	N/A	0.01	N/A
	Transm.[d]	189.0	1802.5	188.9	2085.3	188.8	2015.9	157.8	1839.67
	ASC[e]	84.8		79.8		70.4		67.9	
partitioned ($B = 19$)	W_{off}	464.3	1696.3 (38.4)	478.8	1687.9 (39.7)	400.8	1521.3 (22.4)	412.4	1519.4 (23.7)
	OCGT	268.0	7.7	267.1	7.8	230.5	9.6	226.1	9.8
	CCGT	34.3	46.6	32.9	51.4	24.7	23.4	25.5	26.0
	Li-Ion	0.0	N/A	0.0	N/A	0.01	N/A	0.0	N/A
	Transm.	124.3	1359.3	124.4	1371.7	116.3	1319.6	115.8	1306.9
	ASC	74.2		76.3		63.3		64.7	

[a] K denotes the system-wide capacity of a given technology (incl. legacy capacity), resulting from the optimization exercise and it is expressed in energy units. For instance, capacities of generation technologies (e.g., offshore wind, OCGT, CCGT) are reported in GW. For lithium-ion storage (Li-Ion), the same quantity is expressed in GWh, while transmission capacities are expressed in TWkm.

[b] p denotes the amount of electricity produced (for generation technologies) or transported (for transmission technologies) across a full year. Values are expressed in TWh.

[c] Values in parentheses represent offshore wind curtailment volumes (expressed in the same units as p).

[d] In this table, both electricity transmission technologies (i.e., AC and DC) are aggregated into one entry.

[e] ASC stands for "annualized (total) system cost", is expressed in billion € and represents the objective function of the expansion planning stage.

schemes (recall that $PROD$ is by design selecting the locations with the highest capacity factors in all $B = 19$ regions). More specifically, the average capacity factors for the $PROD$ set of $k = 353$ sites are 42.3% and 43.8% (2010 and 2014, respectively), compared to 40.9% (during 2010) and 42.3% (during 2014) for the $COMP$ set of locations. This time, however, the $PROD$ deployment pattern also exploits a great deal of resource diversity itself, which leads to significantly mitigated dispatchable capacity and generation requirements compared to the unpartitioned $PROD$ case. The $COMP$ siting scheme enables, even in these conditions, an overall capacity reduction of dispatchable units (i.e., of 2.4 GW and 3.6 GW in 2010 and 2014, respectively) compared to $PROD$, which indicates that the complementarity-based siting method still manages to provide a set of sites that decreases the peak residual demand across the system. However, power generation from VOM-intensive dispatchable power plants is now used to make up for the offshore wind feed-in deficit, thus resulting in increased O&M expenditures compounding the additional capital costs due to wind offshore deployments. Finally, no significant differences can be seen in terms of transmission capacity or transmitted volumes. These results suggest that, as opposed to the unpartitioned scenario, $COMP$ slightly underperforms compared with a siting strategy that assumes the deployment of the most productive offshore sites across the 19 EEZs.

5.3. Sensitivity analysis

In this section, a sensitivity analysis is performed in order to evaluate the robustness of results obtained for the partitioned deployment patterns with respect to offshore wind cost assumptions and inter-annual weather variability.

5.3.1. Impact of offshore wind cost assumptions

In view of recent offshore wind economic projections suggesting that costs are likely to decrease substantially by 2050 [55] and considering the small difference between annualized system costs reported in Table 2 for the $PROD$ and $COMP$ schemes (especially for the partitioned set-ups), evaluating the sensitivity of these results to the economic assumptions laid out in Table 1 is warranted. More precisely, the outcomes of the partitioned $PROD$ and $COMP$ schemes are used in CEP set-ups where the capital expenditure of offshore wind is varied between 25% and 125% of the reference cost, by increments of 25%. The results of this experiment are gathered in Fig. 8, where the red and blue markers represent the relative difference (in percentage points) between the objectives of $PROD$- and $COMP$-based runs (a positive value indicates higher costs for the latter) for the 2010 and 2014 weather years, respectively.

It is clear from Fig. 8 that $COMP$-based power system designs are consistently more expensive than their $PROD$ counterparts, regardless of the offshore wind cost. The relative difference between the sizing objectives decreases steadily as the value of the cost multiplier decreases and falls below 2% for both weather years considered, when offshore wind CAPEX is assumed to be only 25% of the reference value. Overall, the $COMP$ schemes lead to system designs that are 1.37% to 2.51% and 1.83% to 2.88% more expensive than their $PROD$ counterparts for the 2014 and 2010 weather years, respectively. The main reason behind $PROD$ consistently leading to cheaper system configurations is the fact that, regardless of the offshore wind cost, the total cost of $COMP$-based system designs is offset by additional offshore wind capacity deployments. As already discussed in Section 5.2.2, this outcome is driven by lower average capacity factors for the $COMP$ sites compared to the ones corresponding to the $PROD$ sets of locations.

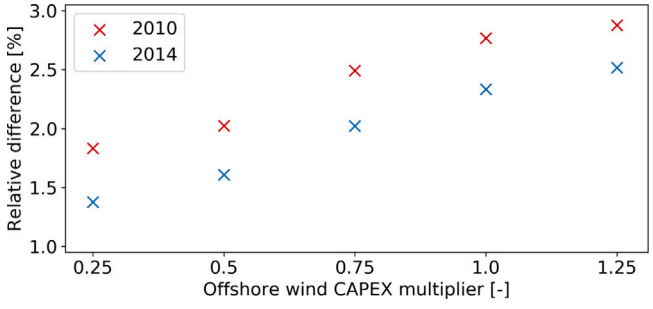

Fig. 8. Relative differences in annualized system costs achieved by expansion planning instances using the outcomes of partitioned ($B = 19$) $COMP$ and $PROD$ siting schemes, for different offshore wind CAPEX multiplicative factors. The analysis is carried out for two weather years (i.e., 2010 and 2014).

Table 3
Breakdown of installed capacities and costs per technology for the partitioned $PROD$- and $COMP$-based system designs obtained for a sizing problem instance with a time horizon of ten years (corresponding to the ten weather years used in the siting stage, namely 2010–2019).

Scheme	ASC		OCGT	CCGT	W_{off}	Transm.
$PROD$	722.68 (b€)	K (GW/TWkm)	291.3	36.4	435.7	129.4
		CAPEX (b€)	106.6	17.4	420.6	41.7
		p (TWh)	88.0	590.6	16512.5	14270.5
		OPEX (b€)	8.2	41.1	0.0	0.0
$COMP$	740.22 (b€)	K (GW/TWkm)	288.4	36.6	444.3	129.4
		CAPEX (b€)	105.6	17.5	431.4	41.7
		p (TWh)	80.4	696.3	16334.0	14147.4
		OPEX (b€)	7.5	48.4	0.0	0.0

5.3.2. Impact of inter-annual weather variability

The variance in the sizing outcomes obtained for problem instances with a time horizon of one year (shown in Fig. 7) supports previous findings suggesting that inter-annual weather variability may have a substantial impact on the cost of operating power systems with high shares of RES-based generation [56]. Consequently, this experiment seeks to evaluate the performance of power system designs obtained with the partitioned $PROD$ and $COMP$ schemes when the full time series of weather data leveraged in the siting stage (i.e., 2010–2019) is used to instantiate the CEP problem that sizes the system.

The figures in Table 3 indicate that the intuition provided by the sizing runs relying on extreme weather years (see Section 5.2.2) still holds when the inter-annual variability of the offshore wind resource is properly accounted for. More specifically, the system configuration based on the $COMP$ siting strategy is 2.4% more expensive than the one relying on the $PROD$ deployment scheme. Two main factors are behind this cost difference. First, the partitioned $PROD$ siting scheme naturally yields a collection of very productive offshore wind sites. Indeed, a ten-year average capacity factor of 43.2% is achieved across the 353 sites. Moreover, as previously reported in Section 5.2.2, the partitioned $PROD$ deployment pattern achieves a $COMP$ siting objective that is only 1% lower than that of the $COMP$ deployment pattern. On the other hand, the average capacity factor of the 353 $COMP$ sites is around 41.9%. This drives the investment in an additional 8.6 GW of offshore wind capacity in the $COMP$ system, which represents more than half of the annualized system cost difference between $PROD$ and $COMP$ in Table 3. Second, although the $COMP$ siting scheme leads to a system design with more offshore wind capacity, the slightly inferior capacity factors lead to a generation deficit of 178 TWh across the ten-year optimization horizon. Legacy generation units, e.g., run-of-river or reservoir-based hydro plants, with non-zero operating costs (as opposed to offshore wind generation) and CCGT power plants (with high O&M costs) are used to cover the aforementioned shortfall. In total, the additional operating costs incurred by this shift from offshore wind to other generation technologies account for the remainder of the total cost difference observed between the $PROD$- and $COMP$-based configurations in Table 3.

5.4. Discussion

It is worth pointing out that, even in the most extreme of situations (represented in Fig. 7 by the 2010 unpartitioned set-up), the relative cost difference between system designs using $PROD$ or $COMP$ siting outcomes does not exceed 6%. The reasons for this limited difference are twofold. First, the case study proposed in this paper investigates solely the siting of offshore wind sites. In the ten-year runs detailed in Section 5.3.2, offshore wind represents 38.7% and 45.4% of the Europe-wide total installed capacity and generation volumes, respectively (values for the $COMP$-based run), while the remainder corresponds to power generation, storage and transmission technologies which are modelled in an identical fashion in both $PROD$- and $COMP$-based CEP set-ups. Therefore, the system cost differences identified throughout Section 5.2 should be interpreted accordingly as the economic impact of one offshore wind siting strategy or the other on the design of the power system. Second, it should be emphasized that 135 out of a total of $k = 353$ sited offshore locations (i.e., a share of 38%) belong to the subset of legacy sites. This aspect further explains the relatively limited differences in total system costs as, in practice, only 218 offshore wind locations are being sited via the investigated siting strategies. In other words, at most 218 offshore wind resource profiles can differ between the outcomes of $COMP$ and $PROD$.

An observation consistently made throughout the results section is that $COMP$ outperforms $PROD$ as long as the latter does not fully exploit the resource diversity available across European EEZs (i.e., the unpartitioned set-ups). This suggests that concentrating offshore wind installations in rich, but relatively limited geographical scopes (e.g., the North Sea [57]), while deferring their deployment in regions swept by distinct wind regimes (e.g., the Baltic or Mediterranean areas) could lead to undesirable outcomes. One example of such an outcome would be the heavy deployment of thermal dispatchable capacity that would be required to guarantee system adequacy which, considering the duration of investment cycles in the power sector and unless carbon-neutral fuels can be used, would lead to investment decisions that are not consistent with the pathways enabling the achievement of ambitious climate targets by 2050 [2].

Another finding in Section 5.2.2 concerns the differences observed between the system configurations leveraging the unpartitioned and partitioned siting schemes, respectively. In particular, the two $COMP$ schemes will be discussed. On the one hand, as the unpartitioned set-up is a relaxation of the partitioned case, the former outperforms the latter in terms of siting scores. Specifically, the $B = 1$ case yields a set of locations covering 99.36% of the time windows, while 95.77% of the time windows are non-critical under the $B = 19$ set-up. Interestingly, the superior siting score of the unpartitioned scheme does not translate into a cheaper system configuration, as observed in Fig. 7, where **x** markers fall below the **o** markers, regardless of the weather year considered. This outcome can be partly explained by the workings of the system adequacy constraint (4s) of the CEP framework, according to which offshore wind (as any other RES technology) can contribute to the provision of firm capacity. More precisely, this constraint is such that system adequacy must be ensured at country-level in order to avoid situations where certain countries excessively depend on electricity imports. Thus, in the partitioned set-up, offshore wind contributes to the provision of firm capacity in all $B = 19$ countries across Europe where capacity could be deployed [7]. On the contrary, ignoring the partitioning constraints (i.e., $B = 1$) results in some countries having less (e.g., Germany, the Netherlands, Norway, etc.) wind deployments compared with the partitioned set-up, as seen in Fig. 2. For those countries, the offshore wind potential (which is proportional to the number of deployed sites) becomes lower than in the partitioned set-up (where more sites were deployed) and, in turn, cannot contribute as much to system adequacy. The two dispatchable power generation technologies sized in the CEP problem (i.e., OCGT and CCGT) become the alternatives for firm capacity (since other RES are not sized in the CEP) and the optimizer ends up deploying additional OCGT capacity

due to its lower cost per unit capacity, thus augmenting the total system cost of the unpartitioned set-up.

Another explanation for the partitioned cases outperforming the unpartitioned ones in terms of system cost pertains to the limited amount of system-related information that is made available to the siting stage, irrespective of the siting strategy considered. An example of such information whose implications are relatively easy to gauge are the network constraints. Recall that the siting stage relies solely on renewable resource and electricity demand data and that the classification of time windows is oblivious to limits on transmission capacity between regions. In consequence, even though the unpartitioned $COMP$ siting scheme leads to a higher siting score than the partitioned case, the CEP stage does not manage to take full advantage of the offshore sites identified in the $B = 1$ set-up. Indeed, on average (across the ten single-year $COMP$ runs reported in Fig. 7), the capacities deployed at 92.2% of the 218 offshore sites selected by the partitioned $COMP$ scheme (excluding legacy sites) exceed 100 MW, while only 73.4% of them exceed the same capacity threshold in the CEP set-up based on the unpartitioned $COMP$ outcome. Most of the unexploited sites in the $B = 1$ scheme are located in the densely deployed areas of Southwestern and Southeastern Europe. From a siting perspective, the wind regimes of these regions are particularly appealing, since they differ from the ones that prevail in the Northern half of the continent [53]. Nevertheless, in this case, the benefits of resource diversity cannot be reaped due to the limited options for electricity transmission between the Iberian peninsula and Central-Western Europe, and between Greece and Central Europe.

6. Conclusion

In this paper, a realistic case study evaluating the role that offshore wind power plants may play in the European power system is proposed, with a particular focus on the impact that plant siting strategies have on system design and economics. The paper builds upon a method that combines a siting stage selecting a subset of promising locations for deployment and a capacity expansion framework identifying the power system design that supplies pre-specified demand levels at minimum cost while satisfying technical and policy constraints. In the interest of transparency, an open source tool implementing the two-stage method is also made available [16,17].

Two types of deployment schemes that select sites so as to maximize their aggregate power output and spatiotemporal complementarity, respectively, are analysed. Two variants of these siting schemes are also considered, wherein the number of sites to be selected is specified on a country-by-country basis rather than Europe-wide. A few hundred sites are identified by each scheme using a high resolution grid and ten years of reanalysis data, and these sites are then passed to a capacity expansion planning framework in order to assess the impact of siting decisions on power system design and economics. The framework relies on a stylized model of the European power system where each country corresponds to an electrical bus and includes an array of power generation and storage technologies. The framework seeks to size gas-fired power plants, offshore wind power plants, battery storage and electricity transmission assets and operate the system in order to supply electricity demand levels consistent with current European electricity consumption at minimum cost while reducing carbon dioxide emissions from the power sector by 90% compared with 1990 levels and taking a broad range of legacy assets into account. A detailed sensitivity analysis is also performed in order to evaluate the impact of offshore wind cost assumptions and inter-annual weather variability on system design.

Results show that the $COMP$ scheme yields deployment patterns that have both a much steadier aggregate power output and much lower residual load levels than the $PROD$ scheme if sites are selected without enforcing country-based deployment targets. However, when such constraints are enforced, the siting schemes produce deployment patterns that lead to similar levels of residual load. This suggests that systematically deploying offshore wind sites in the most productive areas of most European countries makes it possible to take full advantage of the diverse wind regimes available in European seas. In addition, power system designs obtained using $COMP$ deployment patterns consistently feature more offshore wind capacity and less dispatchable capacity than $PROD$-based designs. This difference does not always translate into power systems that are cheaper for either of the siting schemes. More precisely, the $COMP$ scheme leads to system designs that are up to 5% cheaper than $PROD$-based ones when sites are selected without enforcing country-based deployment targets. When such targets are enforced, however, the $PROD$ scheme leads to system designs that are consistently 2% cheaper than $COMP$-based ones. The results are shown to hold under a range of offshore wind cost assumptions and are not affected by inter-annual weather variability.

Several directions can be envisioned for refining the analysis. First, integrating the siting of other RES technologies (e.g., onshore wind, solar PV) into the proposed two-stage method would be of interest to evaluate their synergies in supplying European demand at minimal cost. Then, enhancing the network modelling by (i) using a higher spatial resolution and a refined topology, (ii) relying on a better approximation of network flows (e.g., via a DC-OPF model) would improve the accuracy of the analysis. Evaluating the impact of unit commitment costs and constraints on system designs obtained for different siting schemes would also be of interest. Finally, representing the effect of short-term RES uncertainty in dispatch decisions could also provide some insight into the benefits that siting schemes may bring about.

CRediT authorship contribution statement

David Radu: Conceptualization, Methodology, Software, Validation, Investigation, Visualization, Writing – original draft, Writing – review & editing. **Mathias Berger:** Conceptualization, Methodology, Software, Investigation, Writing – original draft, Writing – review & editing. **Antoine Dubois:** Software, Resources, Data curation. **Raphaël Fonteneau:** Conceptualization, Methodology. **Hrvoje Pandžić:** Investigation, Supervision. **Yury Dvorkin:** Investigation, Supervision. **Quentin Louveaux:** Methodology. **Damien Ernst:** Conceptualization, Supervision, Funding acquisition.

Declaration of competing interest

The authors declare that they have no known competing financial interests or personal relationships that could have appeared to influence the work reported in this paper.

Acknowledgments

The authors gratefully acknowledge the support of the Belgian Federal Government and its Energy Transition Fund, under the REMI project.

Appendix A. Supplementary data

Supplementary material related to this article can be found online at https://doi.org/10.1016/j.apenergy.2021.117700.

References

[1] International Energy Agency (IEA). Renewables 2020 data explorer. 2020, https://www.iea.org/articles/renewables-2020-data-explorer.

[2] Net Zero By 2050 - a Roadmap for the Global Energy Sector. Tech. rep., International Energy Agency; 2021, https://www.iea.org/reports/net-zero-by-2050.

[3] Segreto M, Principe L, Desormeaux A, Torre M, Tomassetti L, Tratzi P, et al. Trends in social acceptance of renewable energy across Europe—A literature review. Int J Environ Res Public Health 2020;17(24). http://dx.doi.org/10.3390/ijerph17249161.

[4] Renewable Power Generation Costs in 2019. Tech. rep., International Renewable Energy Agency; 2020, https://www.irena.org/publications/2020/Jun/Renewable-Power-Costs-in-2019.

[5] Badger J, Bauwens I, Casso P, Davis N, Hahmann A, Bo Krohn Hansen S, et al. Global wind atlas 3.0. 2021, https://globalwindatlas.info/.

[6] A Clean Planet for All - a European Strategic Long-Term Vision for a Prosperous, Modern, Competitive and Climate Neutral Economy. Tech. rep., European Commission; 2018, https://ec.europa.eu/clima/policies/strategies/2050_en.

[7] Freeman K, Frost C, Hundleby G, Roberts A, Valpy B, Holttinen H, et al. Our Energy, Our Future - how Offshore Wind Will Help Europe To Go Carbon-Neutral. Tech. rep., WindEurope; 2019, https://windeurope.org/wp-content/uploads/files/about-wind/reports/WindEurope-Our-Energy-Our-Future.pdf.

[8] Engeland K, Borga M, Creutin J-D, François B, Ramos M-H, Vidal J-P. Space-time variability of climate variables and intermittent renewable electricity production - a review. Renew Sustain Energy Rev 2017;79:600–17. http://dx.doi.org/10.1016/j.rser.2017.05.046.

[9] Geth F, Brijs T, Kathan J, Driesen J, Belmans R. An overview of large-scale stationary electricity storage plants in Europe: Current status and new developments. Renew Sustain Energy Rev 2015;52:1212–27. http://dx.doi.org/10.1016/j.rser.2015.07.145.

[10] Stenclik D, Denholm P, Chalamala B. Maintaining balance: The increasing role of energy storage for renewable integration. IEEE Power Energy Mag 2017;15(6):31–9. http://dx.doi.org/10.1109/MPE.2017.2729098.

[11] O'Connell N, Pinson P, Madsen H, O'Malley M. Benefits and challenges of electrical demand response: A critical review. Renew Sustain Energy Rev 2014;39:686–99. http://dx.doi.org/10.1016/j.rser.2014.07.098.

[12] Milligan MR, Artig R. Choosing Wind Power Plant Locations and Sizes Based on Electric Reliability Measures using Multiple-Year Wind Speed Measurements. Tech. Rep. CP-500-26724, NREL; 1999, https://www.osti.gov/biblio/750939.

[13] Giebel G. On the Benefits of Distributed Generation of Wind Energy in Europe (Ph.D. Thesis), Germany: University of Oldenburg; 2001.

[14] Jurasz J, Canales F, Kies A, Guezgouz M, Beluco A. A review on the complementarity of renewable energy sources: Concept, metrics, application and future research directions. Sol Energy 2020;195:703–24. http://dx.doi.org/10.1016/j.solener.2019.11.087.

[15] MacDonald A, Clack C, Alexander A, Dunbar A, Wilczak J, Xie Y. Future cost-competitive electricity systems and their impact on US CO_2 emissions. Nature Clim Change 2016;6. http://dx.doi.org/10.1038/NCLIMATE2921.

[16] Radu D, Berger M. Resite - a tool for RES siting leveraging resource complementarity,

[17] Dubois A, Radu D, Berger M. Replan - a tool for bulk energy systems planning and analysis,

[18] Berger M, Radu D, Fonteneau R, Henry R, Glavic M, Fettweis X, et al. Critical time windows for renewable resource complementarity assessment. Energy 2020;198. http://dx.doi.org/10.1016/j.energy.2020.117308, https://www.sciencedirect.com/science/article/abs/pii/S0360544220304151.

[19] European Centre for Medium-Range Weather Forecasts - ECMWF. Copernicus knowledge base - ERA5 data documentation. 2018, https://confluence.ecmwf.int//display/CKB/.

[20] Pfenninger S, Hawkes A, Keirstead J. Energy systems modeling for twenty-first century energy challenges. Renew Sustain Energy Rev 2014;33:74–86. http://dx.doi.org/10.1016/j.rser.2014.02.003, http://www.sciencedirect.com/science/article/pii/S1364032114000872.

[21] Krishnan V, Cole W. Evaluating the value of high spatial resolution in national Capacity Expansion Models using ReEDS, in: 2016 IEEE PES General Meeting.

[22] Frysztacki MM, Hörsch J, Hagenmeyer V, Brown T. The strong effect of network resolution on electricity system models with high shares of wind and solar. Appl Energy 2021;291:116726. http://dx.doi.org/10.1016/j.apenergy.2021.116726, https://www.sciencedirect.com/science/article/pii/S0306261921002439.

[23] Jerez S, Thais F, Tobin I, Wild M, Colette A, Yiou P, et al. The CLIMIX model: A tool to create and evaluate spatially-resolved scenarios of photovoltaic and wind power development. Renew Sustain Energy Rev 2015;42:1–15. http://dx.doi.org/10.1016/j.rser.2014.09.041.

[24] Becker R, Thrän D. Optimal siting of wind farms in wind energy dominated power systems. Energies 2018;11(4):978. http://dx.doi.org/10.3390/en11040978.

[25] Musselman A, Thomas VM, Boland N, Nazzal D. Optimizing wind farm siting to reduce power system impacts of wind variability. Wind Energy 2019;22(7):894–907. http://dx.doi.org/10.1002/we.2328.

[26] Hu J, Harmsen R, Crijns-Graus W, Worrell E. Geographical optimization of variable renewable energy capacity in China using modern portfolio theory. Appl Energy 2019;253:113614. http://dx.doi.org/10.1016/j.apenergy.2019.113614.

[27] Berger M, Radu D, Dubois A, Dvorkin Y, Pandzic H, Louveaux Q, et al. Siting renewable power generation assets with combinatorial optimisation. Optim Lett 2021. https://link.springer.com/article/10.1007/s11590-021-01795-0.

[28] Koltsaklis NE, Dagoumas AS. State-of-the-art generation exp. planning: A review. Appl Energy 2018;230. http://dx.doi.org/10.1016/j.apenergy.2018.08.087.

[29] Baringo L, Conejo AJ. Strategic wind power investment. IEEE Trans Power Syst 2014;29(3):1250–60. http://dx.doi.org/10.1109/TPWRS.2013.2292859.

[30] Munoz FD, Hobbs BF, Ho JL, Kasina S. An engineering-economic approach to transmission planning under market and regulatory uncertainties: WECC case study. IEEE Trans Power Syst 2014;29(1):307–17. http://dx.doi.org/10.1109/TPWRS.2013.2279654.

[31] Zappa W, Junginger M, van den Broek M. Is a 100% renewable European power system feasible by 2050? Appl Energy 2019;233–234:1027–50. http://dx.doi.org/10.1016/j.apenergy.2018.08.109.

[32] Kotzur L, Markewitz P, Robinius M, Stolten D. Impact of different time series aggregation methods on optimal energy system design. Renew Energy 2018;117:474–87. http://dx.doi.org/10.1016/j.renene.2017.10.017.

[33] Wu G, Deshmukh R, Ndhlukulac K, Radojicic T, Reilly-Moman J, Phadke A, et al. Strategic siting and regional grid interconnections key to low-carbon futures in African countries. Proc Natl Acad Sci 2017;114. http://dx.doi.org/10.1073/pnas.1611845114.

[34] Zappa W, van den Broek M. Analysing the potential of integrating wind and solar power in Europe using spatial optimisation under various scenarios. Renew Sustain Energy Rev 2018;94. http://dx.doi.org/10.1016/j.rser.2018.05.071.

[35] Bertsimas D, Tsitsiklis J. Simulated annealing. Stat Sci 1993;8(1):10–5. http://dx.doi.org/10.1214/ss/1177011077.

[36] Mertens T, Bruninx K, Duerinck J, Delarue E. The impact of planning reserve margins and demand uncertainty in generation expansion models. In: IAEE Proceedings; 2018. https://www.mech.kuleuven.be/en/tme/research/energy_environment/Pdf/wp-en2018-16.

[37] Ensslin C, Milligan M, Holttinen H, O'Malley M, Keane A. Current Methods To Calculate Capacity Credit of Wind Power. IEA collaboration; 2008, p. 1–3. http://dx.doi.org/10.1109/PES.2008.4596006.

[38] Brown T, Hörsch J, Schlachtberger D. PyPSA: Python for power system analysis. J Open Res Softw 2018;6. http://dx.doi.org/10.5334/jors.188, arXiv:1707.09913.

[39] Staffell I, Pfenninger S. Using bias-corrected reanalysis to simulate current and future wind power output. Energy 2016;114:1224–39. http://dx.doi.org/10.1016/j.energy.2016.08.068, http://www.sciencedirect.com/science/article/pii/S0360544216311811.

[40] Pfenninger S, Staffell I. Long-term patterns of European PV output using 30 years of validated hourly reanalysis and satellite data. Energy 2016;114:1251–65. http://dx.doi.org/10.1016/j.energy.2016.08.060, http://www.sciencedirect.com/science/article/pii/S0360544216311744.

[41] International Electrotechnical Commission. IEC 61400-1:2019: Wind Energy Generation Systems - Part 1: Design Requirements. 2019, https://webstore.iec.ch/publication/26423.

[42] Norgaard P, Holttinen H. A multi-turbine power curve approach. 2004.

[43] Clean Energy Transition - Technologies and Innovations, Accompanying the Report on Progress of Clean Energy Competitiveness. Tech. rep., European Commission; 2020, https://ec.europa.eu/energy/topics/technology-and-innovation/clean-energy-competitiveness_en.

[44] ENTSO-E. Maps & data: TYNDP2018. 2018, https://tyndp.entsoe.eu/maps-data.

[45] Danish Energy Agency. Technology Data for Generation of Electricity and District Heating. 2020, https://ens.dk/en/our-services/projections-and-models/technology-data/technology-data-generation-electricity-and.

[46] ENTSO-E. Power Statistics. 2021, https://www.entsoe.eu/data/power-stats/.

[47] European Commission - Joint Research Centre. The Joint Research Centre Power Plant Database (JRC-PPDB). 2019, https://ec.europa.eu/jrc/en/publication/joint-research-centre-power-plant-database-jrc-ppdb.

[48] European Commission - Joint Research Centre. JRC Hydro-power plants database. 2020, https://github.com/energy-modelling-toolkit/hydro-power-database.

[49] Pierrot M. The Wind Power - Wind Energy Market Intelligence. 2020, https://www.thewindpower.net/store_continent_en.php?id_zone=1001.

[50] Wolfe P. Wiki solar - the authority on utility-scale solar power. 2020, https://www.wiki-solar.org/data/index.html.

[51] Beauvais A, Herrero Cangas M, Chevillard N, Heisz M, Labordena M, Rossi R. EU Market Outlook for Solar Power 2019-2023. Tech. rep., Solar Power Europe; 2019, https://www.solarpowereurope.org/eu-market-outlook-for-solar-power-2019-2023/.

[52] Radu D, Dubois A, Berger M. Assessing the economic value of renewable resource complementarity for power systems: a european study - dataset. 2020, https://dox.uliege.be/index.php/s/u6kPFWKRG0GlDqg.

[53] Grams CM, Beerli R, Pfenninger S, Staffell I, Wernli H. Balancing europe's wind-power output through spatial deployment informed by weather regimes. Nature Clim Change 2017;7:557–62. http://dx.doi.org/10.1038/nclimate3338.

[54] Cortesi N, Torralba V, González-Reviriego N, Soret A, Doblas-Reyes FJ. Characterization of european wind speed variability using weather regimes. Clim Dynam 2019;53:4961–76. http://dx.doi.org/10.1007/s00382-019-04839-5.

[55] Wiser R, Rand J, Seel J, Beiter P, Baker E, Lantz E, et al. Expert elicitation survey predicts 37% to 49% declines in wind energy costs by 2050. Nat Energy 2021;53:4961–76. http://dx.doi.org/10.1038/s41560-021-00810-z.

[56] Collins S, Deane P, Gallachóir BÓ, Pfenninger S, Staffell I. Impacts of inter-annual wind and solar variations on the European power system. Joule 2018;2(10):2076–90. http://dx.doi.org/10.1016/j.joule.2018.06.020, https://www.sciencedirect.com/science/article/pii/S254243511830285X.

[57] Towards the First Hub-and-Spoke Project. Tech. rep., North Sea Wind Power Hub Consortium; 2021, https://northseawindpowerhub.eu/knowledge/towards-the-first-hub-and-spoke-project.